



**HAL**  
open science

# A discrete de Rham discretization of interface diffusion problems with application to the Leaky Dielectric Model

Daniele Di Pietro, Simon Mendez, Aurelio Spadotto

## ► To cite this version:

Daniele Di Pietro, Simon Mendez, Aurelio Spadotto. A discrete de Rham discretization of interface diffusion problems with application to the Leaky Dielectric Model. *Journal of Computational Physics*, 2025, 530, pp.113920. <10.1016/j.jcp.2025.113920>. <hal-05081625>

**HAL Id: hal-05081625**

**<https://hal.science/hal-05081625v1>**

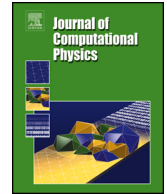
Submitted on 23 May 2025

HAL is a multi-disciplinary open access archive for the deposit and dissemination of scientific research documents, whether they are published or not. The documents may come from teaching and research institutions in France or abroad, or from public or private research centers.

L'archive ouverte pluridisciplinaire HAL, est destinée au dépôt et à la diffusion de documents scientifiques de niveau recherche, publiés ou non, émanant des établissements d'enseignement et de recherche français ou étrangers, des laboratoires publics ou privés.



Distributed under a Creative Commons CC BY-NC-ND 4.0 - Attribution - Non-commercial use - No Derivative Works - International License



# A discrete de Rham discretization of interface diffusion problems with application to the Leaky Dielectric Model

Daniele A. Di Pietro , Simon Mendez , Aurelio E. Spadotto \*

IMAG, Univ. Montpellier, CNRS, Montpellier, France

## ARTICLE INFO

MSC:  
78M10  
65N30  
35J15

### Keywords:

Leaky dielectric model  
Interface diffusion problems  
Discrete de Rham methods  
Polytopal methods  
Weakly enforced interface conditions

## ABSTRACT

Motivated by the study of the electrodynamics of particles, we propose in this work an arbitrary-order discrete de Rham scheme for the treatment of elliptic problems with potential and flux jumps across a fixed interface. The scheme seamlessly supports general elements resulting from the cutting of a background mesh along the interface. Interface conditions are enforced weakly *à la Nitsche*. We provide a rigorous convergence analysis of the scheme for a steady model problem and showcase an application to a physical problem inspired by the Leaky Dielectric Model.

## 1. Introduction

The study of the dynamics of particles in an electric field is motivated by numerous applications. Applying an electric field to cells provides a non-invasive, label-free approach for high-throughput characterization of individual cells [36]. A classical device is the Coulter counter [14], developed in the 1950s and still used in blood analyzers to count and size red blood cells [37] using a DC field. Nowadays, the use of AC fields combined with the versatility of microfluidics makes single-cell microfluidic impedance cytometry a promising technique for multiparametric cell characterization [28]. Other processes in which cells are subjected to an electric field include dielectrophoresis, a common technique used to manipulate or deform cells [27], and electroporation, in which pores are created in the membrane to enable exchange of molecules between the internal and the suspending media [32]. From a more fundamental point of view, subjecting simpler particles like drops or vesicles to electrical fields has revealed fascinating dynamics when the internal and the external fluids have different conductivity and permittivity [41]: symmetry-breaking (rotation of the particle), large transient deformations with sharp edges for vesicles, etc.

Motivated by the problem of the deformation of a drop in a steady electric field [40], G. I. Taylor introduced the so-called Leaky Dielectric Model, in which bulk fluids are assumed to be free of charge, so that the coupling between electric and mechanical phenomena occurs at the interface. Since then, the Leaky Dielectric Model has been shown to provide valuable theoretical insights in the field of electrohydrodynamics of particles [33,41]. In the context of this model, the electrostatic potential is a scalar-valued field which is harmonic in the bulk while, on the droplet interface, it fulfills conditions that express the continuity of current through the membrane as well as a drop in potential called *Galvani potential* [31]. When seeking numerical solutions to this problem, tracking

\* Corresponding author.

E-mail addresses: [daniele.di-pietro@umontpellier.fr](mailto:daniele.di-pietro@umontpellier.fr) (D.A. Di Pietro), [simon.mendez@umontpellier.fr](mailto:simon.mendez@umontpellier.fr) (S. Mendez), [aurelio-edoardo.spadotto@umontpellier.fr](mailto:aurelio-edoardo.spadotto@umontpellier.fr) (A.E. Spadotto).

<https://doi.org/10.1016/j.jcp.2025.113920>

Received 23 September 2024; Received in revised form 23 January 2025; Accepted 6 March 2025

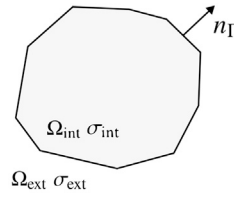


Fig. 1. Configuration for the continuous problem. The polyline can possibly be an approximation to a smooth interface.

the position of the interface by means of an adapted mesh can be challenging and impact on the cost of the simulation. This calls for solutions where the mesh is not redesigned after each displacement of the membrane.

The literature on numerical methods for interface problems is vast, and we will limit ourselves here to works that bear relations with the present approach. A large number of methods rely on a background mesh which is not compliant with the interface, and are therefore referred to as *unfitted*. In the Generalized/Extended Finite Element method [35,34], non-polynomial functions with compact support are added to the discrete space in order to capture the behavior at the interface. In the Immersed Finite Element method [1], the added functions are piecewise polynomials. In the CutFEM method [9], interface conditions are taken into account by using discontinuous basis functions inside the elements cut by the interface and relying on Nitsche's techniques for their enforcement. The CutFEM principles have been extended to the Hybrid High-Order (HHO) method [10,11], which supports much more general element geometries than standard Finite Elements; see [23,20,21,16]. Recently, the ideas underlying HHO methods have been applied in [19,25] to the construction and analysis of discrete de Rham (DDR) sequences in two- and three-space dimensions; see also [6] for an extension to arbitrary dimensions using the language of differential forms. In addition to the support of polytopal meshes and arbitrary order, the DDR approach provides a higher level construction that, on certain element types, can result in spaces that are leaner with respect to their Finite Element counterparts (particularly when serendipity techniques are used [18] and for advanced complexes [8,24]).

In the present work, we consider a method based on meshes obtained by cutting elements crossed by the interface. No special treatment (such as the addition of ad hoc functions) is required for discretization of the diffusion operator on the elements resulting from the cut. This is because the discretization in the bulk hinges on the  $H^1$ -like DDR space of [25], which supports general polygonal or polyhedral meshes. As a result, our method enjoys both the assets of unfitted methods (since cuts can occur at arbitrary locations, making the approximation of the interface totally independent of the background mesh) and of fitted methods (since interface elements do not require a special treatment). The support of general polytopal elements additionally provides an effective means to counter the possible degradation of mesh quality resulting from the cuts, since pathological elements can be merged into neighbors in the spirit of [4,2,30]; see also [29] for an application of these ideas to conforming finite elements. Additionally, the method proposed here can be seamlessly combined with standard (Lagrange) Finite Elements or Finite Element-Finite Volume methods on non-cut elements (such as the ones present in the YALES2BIO platform,<sup>1</sup> whose application to Coulter counters motivated the present effort [38,39]). Interface conditions are enforced weakly through subtly defined terms that ensure consistency; see Remark 5 for further insight into this point. The design of such terms, based on the use of trace reconstructions, is indeed one of the main contributions of the present work. Robustness with respect to the jumps of the diffusion coefficient is obtained by using diffusion-dependent weighted averages in the spirit of [12,22]. To keep the exposition as simple as possible, we focus here on the two-dimensional case with interfaces approximated by closed polygonal chains and consider numerically the case of curved interfaces.

The rest of this work is organized as follows. In Section 2 we state the continuous problem. The discrete setting (mesh, polynomial spaces) is introduced in Section 3. In Section 4 we describe the construction leading to the discrete problem and state the scheme as well as the main results of the analysis. A comprehensive set of numerical tests is carried out in Section 5, while the application to the Leaky Dielectric Model makes the object of Section 6. Finally, the proofs of the stability and error estimates results stated in Section 4.6 are provided in Section 7.

## 2. Continuous setting

To keep the description of the method as simple as possible, we focus on the two-dimensional case. We emphasize, however, that it is possible to extend the present method to three space dimensions in the spirit of [25], as well as to curved approximations of the interface by adapting the techniques of [7,5,42].

Consider an open bounded connected polygonal domain  $\Omega \subset \mathbb{R}^2$  with boundary  $\partial\Omega$ . Let  $\Gamma \subset \Omega$  be a closed non-intersecting polygonal chain such that  $\Gamma \cap \partial\Omega = \emptyset$  (see Fig. 1). The domain is partitioned by  $\Gamma$  into an internal and an external polygonal subdomains, respectively denoted by  $\Omega_{\text{int}}$  and  $\Omega_{\text{ext}}$  in what follows. We denote by  $n_\Gamma$  the unit vector field normal to  $\Gamma$  and pointing out of  $\Omega_{\text{int}}$ .

Given a couple of functions  $v = (v_{\text{int}}, v_{\text{ext}})$  with  $v_\bullet : \Omega_\bullet \rightarrow \mathbb{R}$  for  $\bullet \in \{\text{int}, \text{ext}\}$ , each smooth enough to admit a trace on  $\Gamma$ , we define the following interface jump operator:

$$[v]_\Gamma := v_{\text{int}} - v_{\text{ext}}. \quad (1)$$

<sup>1</sup> See <https://imag.umontpellier.fr/~yales2bio/>.

When applied to couples of vector-valued functions, the jump operator acts component-wise. In what follows, whenever needed, we tacitly identify  $v$  with the function  $v_{\text{int}} I_{\Omega_{\text{int}}} + v_{\text{ext}} I_{\Omega_{\text{ext}}} : \Omega \setminus \Gamma \rightarrow \mathbb{R}$ , where  $I_{\Omega_{\bullet}}$  is the characteristic function of  $\Omega_{\bullet}$ . Consider a region-wise constant diffusion coefficient  $\sigma : \Omega \setminus \Gamma \rightarrow \mathbb{R}$  such that  $\sigma|_{\Omega_{\text{int}}} \equiv \sigma_{\text{int}} > 0$  and  $\sigma|_{\Omega_{\text{ext}}} \equiv \sigma_{\text{ext}} > 0$ . Let  $f : \Omega \setminus \Gamma \rightarrow \mathbb{R}$ ,  $\Phi_{\Gamma} : \Gamma \rightarrow \mathbb{R}^2$ , and  $J_{\Gamma} : \Gamma \rightarrow \mathbb{R}$  be given functions, which we assume smooth enough for the following discussion to make sense. We consider the problem of finding the couple of scalar-valued functions  $u = (u_{\text{int}}, u_{\text{ext}})$  with  $u_{\bullet} : \Omega_{\bullet} \rightarrow \mathbb{R}$ ,  $\bullet \in \{\text{int}, \text{ext}\}$ , such that

$$-\nabla \cdot (\sigma_{\bullet} \nabla u_{\bullet}) = f \quad \text{in } \Omega_{\bullet}, \bullet \in \{\text{int}, \text{ext}\}, \quad (2a)$$

$$[u]_{\Gamma} = J_{\Gamma} \quad \text{on } \Gamma, \quad (2b)$$

$$[\sigma \nabla u]_{\Gamma} \cdot n_{\Gamma} = \Phi_{\Gamma} \quad \text{on } \Gamma, \quad (2c)$$

$$u_{\text{ext}} = 0 \quad \text{on } \partial\Omega. \quad (2d)$$

### 3. Discrete setting

#### 3.1. Mesh

We discretize the domain with a polygonal mesh  $(\mathcal{T}_h, \mathcal{E}_h)$  in the sense of [16, Definition 1.4], with  $\mathcal{T}_h$  collecting the mesh elements and  $\mathcal{E}_h$  the mesh edges. We additionally denote by  $\mathcal{V}_h$  the set of vertices collecting the edge endpoints. The mesh is assumed to be fitted to the interface, i.e., there exists a subset  $\mathcal{E}_{\Gamma, h}$  of  $\mathcal{E}_h$  such that  $\Gamma = \bigcup_{E \in \mathcal{E}_{\Gamma, h}} \overline{E}$ .

**Remark 1 (Fitted mesh).** It is important to emphasize that fitted polytopal meshes supported by the present method can simply be obtained cutting the elements of a background mesh along the interface, as in the numerical tests of Sections 5 and 6. This is a major advantage, particularly in the framework of moving interface problems, as it avoids a potentially expensive remeshing step. We also notice that the degradation of mesh quality can also be countered leveraging the support of polytopal elements: whenever an elongated or distorted element results from the cutting, it can be agglomerated into neighboring elements in the spirit of [4, 2, 30] to restore mesh quality.

**Remark 2 (Approximation of the interface).** The approximation of the interface is totally independent of the background mesh. This is important when considering the more general case of curved interfaces, where a finer discretization can be needed. We refer to Remark 8 for further insight into the situation when the interface is refined “faster” than the bulk mesh.

For  $\bullet \in \{\text{int}, \text{ext}\}$ , we denote by  $\mathcal{T}_h^{\bullet}$ ,  $\mathcal{E}_h^{\bullet}$ , and  $\mathcal{V}_h^{\bullet}$ , respectively, the sets of elements, edges, and vertices contained in  $\overline{\Omega_{\bullet}}$ . Notice that edges that lie on  $\Gamma$  belong to both  $\mathcal{E}_h^{\text{int}}$  and  $\mathcal{E}_h^{\text{ext}}$ , and similarly for vertices. For any element  $T \in \mathcal{T}_h$ , we denote by  $\mathcal{E}_T$  the set collecting its edges. Symmetrically, the set of elements sharing one edge  $E \in \mathcal{E}_h$  is denoted by  $\mathcal{T}_E$ . For each edge  $E \in \mathcal{E}_h$ , we fix once and for all a unit normal vector  $n_E$  and, for any  $T \in \mathcal{T}_E$ , we denote by  $\omega_{TE} \in \{-1, 1\}$  the relative orientation of  $E$  with respect to  $T$ , such that  $\omega_{TE} n_E$  points out of  $T$ .

In what follows, we assume that the mesh we are working on belongs to a regular sequence in the sense of [16, Definition 1.9]. Given a mesh element or edge  $X \in \mathcal{T}_h \cup \mathcal{E}_h$ , we denote by  $h_X$  its diameter, so that  $h = \max_{T \in \mathcal{T}_h} h_T$ . We will abbreviate by  $a \lesssim b$  the inequality  $a \leq Cb$  with  $C$  independent of  $h$ ,  $\sigma$  and, for local inequalities, the corresponding element or edge. Further details on the dependence of the hidden constants will be provided when appropriate.

#### 3.2. Polynomial spaces

Given  $X \in \mathcal{T}_h \cup \mathcal{E}_h$  and an integer  $m \geq 0$ , we denote by  $\mathcal{P}^m(X)$  the space spanned by the restriction of polynomials of the space variables to  $X$  and by  $\mathcal{P}_X^m$  the corresponding  $L^2$ -orthogonal projector. We conventionally set  $\mathcal{P}^{-1}(X) := \{0\}$ . For all  $T \in \mathcal{T}_h$ , we will also need the space

$$\mathcal{R}^{c, m}(T) := (x - x_T) \mathcal{P}^{m-1}(T),$$

where  $x_T$  is a point inside  $T$  at a distance from its boundary comparable to  $h_T$ . It can be proved that the divergence from  $\mathcal{R}^{c, m}(T)$  to  $\mathcal{P}^{m-1}(T)$  is an isomorphism; cf. [3, Corollary 7.3].

At the global level, we will need the broken polynomial space

$$\mathcal{P}^m(\mathcal{T}_h) := \{v \in L^2(\Omega) : v|_T \in \mathcal{P}^m(T) \text{ for all } T \in \mathcal{T}_h\}.$$

## 4. Discrete problem

### 4.1. Discrete space

For any  $k \geq 0$  and  $\bullet \in \{\text{int}, \text{ext}\}$ , we let

$$\underline{V}_{\bullet,h}^k := \left\{ \underline{v}_h = ((v_T)_{T \in \mathcal{T}_h^\bullet}, (v_E)_{E \in \mathcal{E}_h^\bullet}, (v_V)_{V \in \mathcal{V}_h^\bullet}) : \begin{aligned} v_T &\in \mathcal{P}^{k-1}(T) \text{ for all } T \in \mathcal{T}_h^\bullet, \\ v_E &\in \mathcal{P}^{k-1}(E) \text{ for all } E \in \mathcal{E}_h^\bullet, \\ v_V &\in \mathbb{R} \text{ for all } V \in \mathcal{V}_h^\bullet. \end{aligned} \right\}.$$

We consider the discrete space

$$\underline{V}_h^k := \underline{V}_{\text{int},h}^k \times \underline{V}_{\text{ext},h}^k,$$

as well as its subspace  $\underline{V}_{h,0}^k$  with edge and vertex values vanishing on  $\partial\Omega$ .

The interpolator  $\underline{I}_h^k : C^0(\overline{\Omega}_{\text{int}}) \times C^0(\overline{\Omega}_{\text{ext}}) \rightarrow \underline{V}_h^k$  is such that, for all  $v = (v_{\text{int}}, v_{\text{ext}}) \in C^0(\overline{\Omega}_{\text{int}}) \times C^0(\overline{\Omega}_{\text{ext}})$ ,

$$\underline{I}_h^k v := (\underline{I}_{\text{int},h}^k v_{\text{int}}, \underline{I}_{\text{ext},h}^k v_{\text{ext}}),$$

where, for  $\bullet \in \{\text{int}, \text{ext}\}$ ,

$$\underline{I}_{\bullet,h}^k v_\bullet := ((\pi_T^{k-1} v_\bullet)_{T \in \mathcal{T}_h^\bullet}, (\pi_E^{k-1} v_\bullet)_{E \in \mathcal{E}_h^\bullet}, (v_\bullet(x_V))_{V \in \mathcal{V}_h^\bullet}).$$

For all  $T \in \mathcal{T}_h$ , we respectively denote the restrictions of  $\underline{V}_h^k$ ,  $\underline{v}_h \in \underline{V}_h^k$ , and  $\underline{I}_h^k$  to  $T$  by  $\underline{V}_T^k$ ,  $\underline{v}_T \in \underline{V}_T^k$ , and  $\underline{I}_T^k$ . Such restrictions are obtained collecting the polynomial components on  $T$  and its boundary. More specifically, since every mesh element  $T$  is contained in one and only one subdomain  $\mathcal{T}_h^\bullet$ ,  $\bullet \in \{\text{int}, \text{ext}\}$ , when restricting a vector of polynomials  $\underline{v}_h \in \underline{V}_h^k$  to  $T$ , all the components of the local vector  $\underline{v}_T = (v_T, (v_E)_{E \in \mathcal{E}_T}, (v_V)_{V \in \mathcal{V}_T})$  (with  $\mathcal{V}_T$  denoting the set of vertices of  $T$ ) are extracted from  $\underline{V}_{\bullet,h}^k$ . This removes all possible ambiguity for mesh elements such that  $\partial T \cap \Gamma \neq \emptyset$ .

### 4.2. Element gradient and potential

For any  $T \in \mathcal{T}_h$ , any  $\underline{v}_T \in \underline{V}_T^k$ , and any  $E \in \mathcal{E}_T$ , we let the edge potential  $v_{TE}$  be the unique function in  $\mathcal{P}^{k+1}(E)$  such that

$$v_{TE}(x_V) = v_V \text{ for any endpoint } V \text{ of } E \text{ and } \pi_E^{k-1} v_{TE} = v_E.$$

**Remark 3 (Edge potential).** Clearly,  $v_{TE} \equiv 0$  whenever  $E \subset \partial\Omega$  is a boundary edge and  $\underline{v}_h \in \underline{V}_{h,0}^k$ . On the other hand, when  $E \subset (\partial T_1 \cap \partial T_2) \setminus \Gamma$  is an internal edge that does not lie on the interface, the value of the edge potential does not depend on the element, i.e.,  $v_{T_1 E} = v_{T_2 E}$ .

We define the discrete gradient  $G_T^k : \underline{V}_T^k \rightarrow \mathcal{P}^k(T)^2$  and potential  $p_T^{k+1} : \underline{V}_T^k \rightarrow \mathcal{P}^{k+1}(T)$  such that, for all  $\underline{v}_T \in \underline{V}_T^k$ ,

$$\begin{aligned} \int_T G_T^k \underline{v}_T \cdot \tau &= - \int_T v_T (\nabla \cdot \tau) + \sum_{E \in \mathcal{E}_T} \omega_{TE} \int_E v_{TE} (\tau \cdot n_E) \quad \forall \tau \in \mathcal{P}^k(T)^2, \\ \int_T p_T^{k+1} \underline{v}_T (\nabla \cdot \tau) &= - \int_T G_T^k \underline{v}_T \cdot \tau + \sum_{E \in \mathcal{E}_T} \omega_{TE} \int_E v_{TE} (\tau \cdot n_E) \quad \forall \tau \in \mathcal{R}^{c,k+2}(T). \end{aligned} \quad (3)$$

**Remark 4 (Validity of (3)).** Following [25, Remark 17], the relation (3) actually holds for all  $\tau \in \mathcal{P}^k(T)^2 + \mathcal{R}^{c,k+2}(T)$ .

Accounting for the previous remark, we notice that, integrating by parts the left-hand side of (3) and rearranging, we have, for all  $(\underline{v}_T, \tau) \in \underline{V}_T^k \times (\mathcal{P}^k(T)^2 + \mathcal{R}^{c,k+2}(T))$ ,

$$\int_T \nabla p_T^{k+1} \underline{v}_T \cdot \tau = \int_T G_T^k \underline{v}_T \cdot \tau + \sum_{E \in \mathcal{E}_T} \omega_{TE} \int_E (p_T^{k+1} \underline{v}_T - v_{TE}) (\tau \cdot n_E). \quad (4)$$

Selecting  $\tau = \nabla p_T^{k+1} \underline{v}_T$  (this is possible since  $\nabla p_T^{k+1} \underline{v}_T \in \mathcal{P}^k(T)^d$ ) in the above expression, using Cauchy–Schwarz,  $(2, \infty, 2)$ -Hölder, and trace inequalities along with  $\|n_E\|_{L^\infty(E)^2} \leq 1$  in the right-hand side, and simplifying, we get

$$\|\nabla p_T^{k+1} \underline{v}_T\|_{L^2(T)^2} \lesssim \left( \|G_T^k \underline{v}_T\|_{L^2(T)^2}^2 + h_T^{-1} \sum_{E \in \mathcal{E}_T} \|p_T^{k+1} \underline{v}_T - v_{TE}\|_{L^2(E)}^2 \right)^{1/2}. \quad (5)$$

Let  $v \in H^{r+2}(T)$  for some  $r \in \{0, \dots, k\}$  and set  $\hat{v}_T := \underline{I}_T^k v$ . Using the techniques of [25], where the three-dimensional case is considered, it can be proved that

$$\|\hat{v}_{TE} - v\|_{L^2(E)} \lesssim h_T^{r+3/2} |v|_{H^{r+2}(T)} \quad \forall E \in \mathcal{E}_T, \quad (6)$$

$$\|G_T^k \hat{v}_T - \nabla v\|_{L^2(T)^2} + h_T^{1/2} \|G_T^k \hat{v}_T - \nabla v\|_{L^2(\partial T)^2} \lesssim h_T^{r+1} |v|_{H^{r+2}(T)}, \quad (7)$$

$$\|p_T^{k+1} \hat{v}_T - v\|_{L^2(T)} + h_T^{1/2} \|p_T^{k+1} \hat{v}_T - v\|_{L^2(\partial T)} \lesssim h_T^{r+2} |v|_{H^{r+2}(T)}. \quad (8)$$

For future use, we also define the global discrete gradient operator  $G_h^k : \underline{V}_h^k \rightarrow \mathcal{P}^k(\mathcal{T}_h)^2$  such that, for all  $\underline{v}_h \in \underline{V}_h^k$ ,

$$(G_h^k \underline{v}_h)|_T := G_T^k \underline{v}_T \quad \forall T \in \mathcal{T}_h.$$

### 4.3. Interface trace operators

Let  $E \in \mathcal{E}_{\Gamma,h}$  and denote by  $T_{\text{int}} \in \mathcal{T}_h^{\text{int}}$  and  $T_{\text{ext}} \in \mathcal{T}_h^{\text{ext}}$  the unique elements such that  $E \subset \partial T_{\text{int}} \cap \partial T_{\text{ext}}$ . Notice that, while such elements clearly depend on  $E$ , we do not highlight this dependency in the notation as it will be clear from the context. We define the edge jump  $[\cdot]_E : \underline{V}_h^k \rightarrow \mathcal{P}^{k+1}(E)$  and skewed average  $\{\cdot\}_{\lambda,E} : \underline{V}_h^k \rightarrow \mathcal{P}^{k+1}(E)$  operators such that, for all  $\underline{v}_h \in \underline{V}_h^k$ ,

$$[\underline{v}_h]_E := v_{T_{\text{int}}E} - v_{T_{\text{ext}}E}, \quad \{\underline{v}_h\}_{\lambda,E} := \lambda_{\text{ext}} v_{T_{\text{int}}E} + \lambda_{\text{int}} v_{T_{\text{ext}}E}, \quad (9)$$

with  $\lambda_{\text{int}}$  and  $\lambda_{\text{ext}}$  such that

$$\lambda_{\text{int}} := \frac{\sigma_{\text{ext}}}{\sigma_{\text{int}} + \sigma_{\text{ext}}}, \quad \lambda_{\text{ext}} := \frac{\sigma_{\text{int}}}{\sigma_{\text{int}} + \sigma_{\text{ext}}}. \quad (10)$$

We additionally let, for any vector-valued field  $\Psi$  smooth enough to admit a possibly two-valued trace on  $E$ ,

$$\{\Psi\}_{\lambda,E} := \lambda_{\text{int}} \gamma_{T_{\text{int}}E} \Psi + \lambda_{\text{ext}} \gamma_{T_{\text{ext}}E} \Psi, \quad (11)$$

where  $\gamma_{T,E} \Psi$  denotes the trace of  $\Psi|_T$  on  $E$ .

### 4.4. Discrete problem

Let

$$\sigma_T := \sigma|_T \quad \forall T \in \mathcal{T}_h.$$

Given a user-dependent parameter  $\eta > 0$ , we define the bilinear form  $a_h : \underline{V}_h^k \times \underline{V}_h^k \rightarrow \mathbb{R}$  and the linear form  $\ell_h : \underline{V}_h^k \rightarrow \mathbb{R}$  such that, for all  $(\underline{w}_h, \underline{v}_h) \in \underline{V}_h^k \times \underline{V}_h^k$ ,

$$\begin{aligned} a_h(\underline{w}_h, \underline{v}_h) := & \sum_{T \in \mathcal{T}_h} \left( \int_T \sigma_T G_T^k \underline{w}_T \cdot G_T^k \underline{v}_T + \frac{\sigma_T}{h_T} \sum_{E \in \mathcal{E}_T} \int_E (p_T^{k+1} \underline{w}_T - w_{TE})(p_T^{k+1} \underline{v}_T - v_{TE}) \right) \\ & - \sum_{E \in \mathcal{E}_{\Gamma,h}} \int_E \{\sigma G_h^k \underline{w}_h\}_{\lambda,E} \cdot n_E [\underline{v}_h]_E + \eta \sum_{E \in \mathcal{E}_{\Gamma,h}} \frac{\alpha}{h_E} \int_E [\underline{w}_h]_E [\underline{v}_h]_E, \end{aligned} \quad (12)$$

where

$$\alpha := \frac{2\sigma_{\text{int}}\sigma_{\text{ext}}}{\sigma_{\text{int}} + \sigma_{\text{ext}}} \quad (13)$$

and

$$\ell_h(\underline{v}_h) := \sum_{T \in \mathcal{T}_h} \int_T f p_T^{k+1} \underline{v}_T + \sum_{E \in \mathcal{E}_{\Gamma,h}} \int_E \Phi_\Gamma \{\underline{v}_h\}_{\lambda,E} + \eta \sum_{E \in \mathcal{E}_{\Gamma,h}} \frac{\alpha}{h_E} \int_E J_\Gamma [\underline{v}_h]_E. \quad (14)$$

The discrete problem reads: Find  $\underline{u}_h \in \underline{V}_{h,0}^k$  such that

$$a_h(\underline{u}_h, \underline{v}_h) = \ell_h(\underline{v}_h) \quad \forall \underline{v}_h \in \underline{V}_{h,0}^k. \quad (15)$$

**Remark 5** (*Formulation of the interface terms*). It is worth noticing that the scheme above is not a simple extension of discontinuous Galerkin techniques to the interface problem of Section 2 with the element potential playing the role of the discontinuous solution inside trace operators. On the contrary, such operators use the edge potential in a subtle way, which is required for optimal order consistency; see, in particular, the passages leading to (30) in the proof of Lemma 13 below.

4.5. Energy norm and interface jump seminorm

In order to state the main results of the theoretical analysis of the method, we define on  $\underline{V}_h^k$  the energy norm  $\|\cdot\|_{\text{en},h}$  such that, for all  $\underline{v}_h \in \underline{V}_h^k$ ,

$$\|\underline{v}_h\|_{\text{en},h}^2 := \sum_{T \in \mathcal{T}_h} \sigma_T \left( \|G_T^k \underline{v}_T\|_{L^2(T)}^2 + h_T^{-1} \sum_{E \in \mathcal{E}_T} \|p_T^{k+1} \underline{v}_T - v_{TE}\|_{L^2(E)}^2 \right) + |\underline{v}_h|_{J,h}^2, \tag{16}$$

where the interface jump seminorm is such that

$$|\underline{v}_h|_{J,h}^2 := \sum_{E \in \mathcal{E}_{\Gamma,h}} \frac{\alpha}{h_E} \|[v_h]_E\|_{L^2(E)}^2. \tag{17}$$

**Proposition 6** (Energy norm). *The map  $\|\cdot\|_{\text{en},h}$  defines a norm on  $\underline{V}_{h,0}^k$ .*

**Proof.**  $\|\cdot\|_{\text{en},h}$  is clearly a seminorm, so we only have to prove that, for all  $\underline{v}_h \in \underline{V}_{h,0}^k$ ,  $\|\underline{v}_h\|_{\text{en},h} = 0$  implies  $\underline{v}_h = \underline{0}$ . The condition  $\|\underline{v}_h\|_{\text{en},h} = 0$  implies: (i) for all  $T \in \mathcal{T}_h$ ,  $G_T^k \underline{v}_T = 0$  and  $(p_T^{k+1} \underline{v}_T)|_E = v_{TE}$  for all  $E \in \mathcal{E}_T$  and (ii) for all  $E \in \mathcal{E}_{\Gamma,h}$ ,  $[v_h]_E = 0$ . By (5), point (i) implies, in turn, that  $p_T^{k+1} \underline{v}_T$  is constant on each  $T \in \mathcal{T}_h$ . Since  $v_{TE} = 0$  whenever  $E \in \mathcal{E}_h$  is a boundary edge contained in  $\partial\Omega$  and  $T \in \mathcal{T}_h$  is the unique mesh element to which it belongs,  $p_T^{k+1} \underline{v}_T = 0$ . Proceeding from  $\partial\Omega$  towards the interior of  $\Omega_{\text{ext}}$ , this gives  $p_T^{k+1} \underline{v}_T = 0$  for all  $T \in \mathcal{T}_h^{\text{ext}}$  and  $v_{TE} = 0$  for all  $E \in \mathcal{E}_T$ . These two conditions combined show that all elements, edge, and vertex components of  $\underline{v}_h$  in  $\Omega_{\text{ext}}$  vanish. Since interface jumps vanish as well by point (ii) above, the edge and vertex components of  $\underline{v}_h$  on the interface  $\Gamma$  from the side of  $\Omega_{\text{int}}$  are zero. The same reasoning as for  $\Omega_{\text{ext}}$  can therefore be applied (proceeding from the interface  $\Gamma$  towards the interior of  $\Omega_{\text{int}}$ ) to show that all elements, edge, and vertex values of  $\underline{v}_h$  in  $\Omega_{\text{int}}$  vanish, thus concluding the proof.  $\square$

4.6. Main results

We recall the following discrete trace inequality valid for any integer  $m \geq 0$ , any  $T \in \mathcal{T}_h$ , and any  $E \in \mathcal{E}_T$ : For all  $\varphi \in \mathcal{P}^m(T)$ ,

$$\|\varphi\|_{L^2(E)} \leq C_{\text{tr}} h_E^{-1/2} \|\varphi\|_{L^2(T)}, \tag{18}$$

where the real number  $C_{\text{tr}} > 0$  only depends on  $m$  and the mesh regularity parameter.

**Lemma 7** (Stability). *Let  $N_\partial := \max_{T \in \mathcal{T}_h} \text{card}(\mathcal{E}_T \cap \mathcal{E}_{\Gamma,h})$  and assume that*

$$\eta > \frac{C_{\text{tr}}^2 N_\partial}{4\epsilon} \tag{19}$$

for some real number  $0 < \epsilon < 1$ . Then, for all  $\underline{v}_h \in \underline{V}_{h,0}^k$ , it holds

$$C_{\text{stab}} \|\underline{v}_h\|_{\text{en},h}^2 \leq a_h(\underline{v}_h, \underline{v}_h), \tag{20}$$

with  $C_{\text{stab}} := \min \left\{ 1 - \epsilon, \eta - \frac{C_{\text{tr}}^2 N_\partial}{4\epsilon} \right\}$ .

**Proof.** See Section 7.1  $\square$

**Remark 8** (Interface elements with a large number of edges). In the context of meshes obtained by cutting an underlying standard triangular mesh (such as the ones considered numerically in Sections 5 and 6), a slight modification of the scheme in the spirit of [13,26] can make it robust in the case where the interface is refined “asymptotically faster” than the bulk mesh. Denote by  $S_h$  the set of triangles of the bulk mesh that are cut by the interface. Let, for all  $S \in S_h$ ,  $\mathcal{E}_{\Gamma,S} := \{E \in \mathcal{E}_{\Gamma,h} : E \subset \partial S\}$ , denote by  $h_S := \sum_{E \in \mathcal{E}_{\Gamma,S}} h_E$  the length of the polyline  $\Gamma_S := \Gamma \cap S$ , and assume that  $h_S \simeq h_S$ ; see Fig. 2. Consider the bilinear and linear forms obtained replacing the last terms in the right-hand sides of (12) and (14) respectively by

$$\eta \sum_{S \in S_h} \frac{\alpha}{h_S} \sum_{E \in \mathcal{E}_{\Gamma,S}} \int [w_h]_E [v_h]_E \text{ and } \eta \sum_{S \in S_h} \frac{\alpha}{h_S} \sum_{E \in \mathcal{E}_{\Gamma,S}} \int J_\Gamma [v_h]_E.$$

Then, using the discrete trace inequality  $\|\varphi\|_{L^2(\partial T)} \leq \tilde{C}_{\text{tr}} h_T^{-1/2} \|\varphi\|_{L^2(T)}$  on the whole boundary of the elements of  $\mathcal{T}_h$  instead of (18) and letting  $|\underline{v}_h|_{J,h}^2 := \sum_{S \in S_h} \sum_{E \in \mathcal{E}_{\Gamma,S}} \frac{\alpha}{h_S} \|[v_h]_E\|_{L^2(E)}^2$  (compare with (17)), one can replace condition (19) with  $\eta > \frac{\tilde{C}_{\text{tr}}^2}{4\epsilon}$ , which no longer depends on the (possibly large) integer  $N_\partial$ .

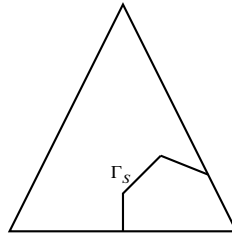


Fig. 2. An example of triangle  $S \in \mathcal{S}_h$  cut by the interface with polyline  $\Gamma_S := \Gamma \cap S$ .

**Theorem 9 (Error estimate).** Let  $u = (u_{\text{int}}, u_{\text{ext}})$  be the weak solution to (2) and  $\underline{u}_h$  solve (15). Under assumption (19), with  $\bar{\sigma} := \max\{\sigma_{\text{int}}, \sigma_{\text{ext}}\}$ , and further assuming that  $u = (u_{\text{int}}, u_{\text{ext}}) \in [C^0(\bar{\Omega}_{\text{int}}) \cap H^{r+2}(\mathcal{T}_h^{\text{int}})] \times [C^0(\bar{\Omega}_{\text{ext}}) \cap H^{r+2}(\mathcal{T}_h^{\text{ext}})]$  for some  $r \in \{0, \dots, k\}$ , it holds

$$\|\underline{u}_h - \underline{I}_h^k u\|_{\text{en},h} \lesssim \bar{\sigma}^{-1/2} h^{r+1} |u|_{H^{r+2}(\mathcal{T}_h)},$$

where  $|\cdot|_{H^{r+2}(\mathcal{T}_h)}$  is the broken  $H^{r+2}$ -seminorm on the mesh  $\mathcal{T}_h$  and the hidden constant depends only on the domain, the stability constant  $C_{\text{stab}}$  in (20), the polynomial degree  $k$ , and the mesh regularity parameter (but is independent of both the meshsize and  $\sigma$ ).

**Proof.** See Section 7.2.  $\square$

**Remark 10 (Robustness in  $\sigma$ ).** Notice that the right-hand side of the above estimate does not depend on the ratio  $\frac{\sigma_{\text{int}}}{\sigma_{\text{ext}}}$ , making it robust in the case of media with highly contrasting properties. Crucial to obtain this robustness property is the use of weighted averages in the spirit of [12,22].

**Remark 11 (Extension to non-piecewise constant diffusion coefficients).** The arguments for stability and convergence can be extended to the case of diffusion coefficients  $\sigma_{\text{int}} : \Omega_{\text{int}} \rightarrow \mathbb{R}$  and  $\sigma_{\text{ext}} : \Omega_{\text{ext}} \rightarrow \mathbb{R}$  that are Lipschitz-continuous on the corresponding subdomain.

## 5. Numerical tests

To numerically assess the theoretical results of Section 4.6, we have implemented in Python the lowest-order version of the scheme corresponding to  $k = 0$ . The implementation is a prototype for the final one in YALES2BIO, and is therefore compliant with the constraints of this software platform.

### 5.1. Square interface

We consider the square domain  $\Omega = (-1/2, 1/2)^2$ , with a square interface

$$\Gamma = \left\{ (x, y) \in [-1/4, 1/4]^2 : |x| = 1/4 \text{ or } |y| = 1/4 \right\}.$$

Since the interface is a polygonal chain, no geometric error is introduced. We consider the following family of solutions  $u = (u_{\text{int}}, u_{\text{ext}})$  parametrized by the ratio  $\frac{\sigma_{\text{ext}}}{\sigma_{\text{int}}}$  and depicted in Fig. 3:

$$u_{\text{int}} = \frac{\sigma_{\text{ext}}}{\sigma_{\text{int}}} (x^2 - y^2), \quad u_{\text{ext}} = x^2 - y^2 \tag{21}$$

with forcing term, (non-homogeneous) boundary conditions, and values for  $J_\Gamma$  and  $\Phi_\Gamma$  inferred from the expression of  $u = (u_{\text{int}}, u_{\text{ext}})$ .

We consider two mesh families, both compliant with the interface. The first sequence is composed of Cartesian orthogonal meshes. The second sequence is obtained from the latter by randomly moving vertices that are not located on the interface within a circle of radius  $\frac{\ell}{5}$ , with  $\ell$  denoting the measure of the sides of the element in the non-deformed mesh; see Fig. 4.

In order to assess the robustness of the method with respect to the ratio  $\frac{\sigma_{\text{int}}}{\sigma_{\text{ext}}}$ , we let this quantity vary in  $\{10^{-6}, 10^{-3}, 10^3, 10^6\}$ . We monitor two measures of the error: the energy norm defined by (16) and the component  $L^2$ -norm  $\|\cdot\|_{0,h}$  defined by [17, Eq. (4.20)], i.e.,

$$\|\underline{v}_h\|_{0,h} := \left( \sum_{T \in \mathcal{T}_h} \|v_T\|_{L^2(T)}^2 + h_T \sum_{E \in \mathcal{E}_T} \|v_E\|_{L^2(E)}^2 \right)^{\frac{1}{2}} \quad \forall \underline{v}_h \in \underline{V}_h^k.$$

In all the cases, the error is normalized with respect to the corresponding norm of the discrete solution. The results that are shown are obtained with  $\eta = 1$ .

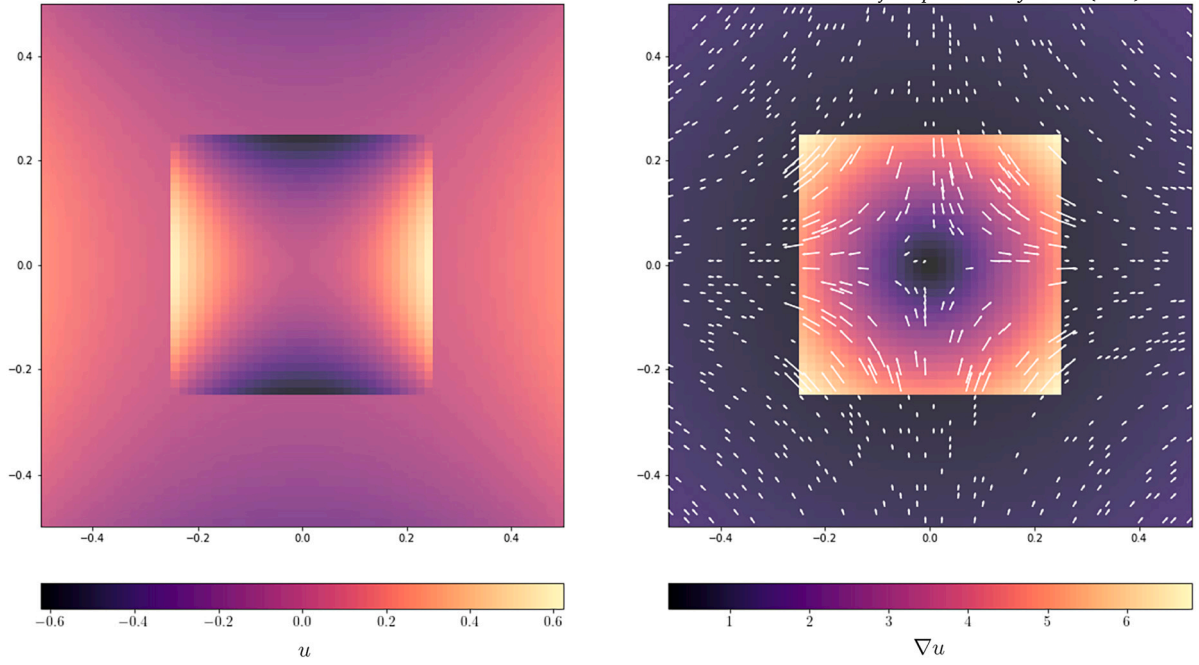


Fig. 3. The exact solution (21) considered in Section 5.1 and its gradient for  $\frac{\sigma_{\text{int}}}{\sigma_{\text{ext}}} = 10^{-1}$ .

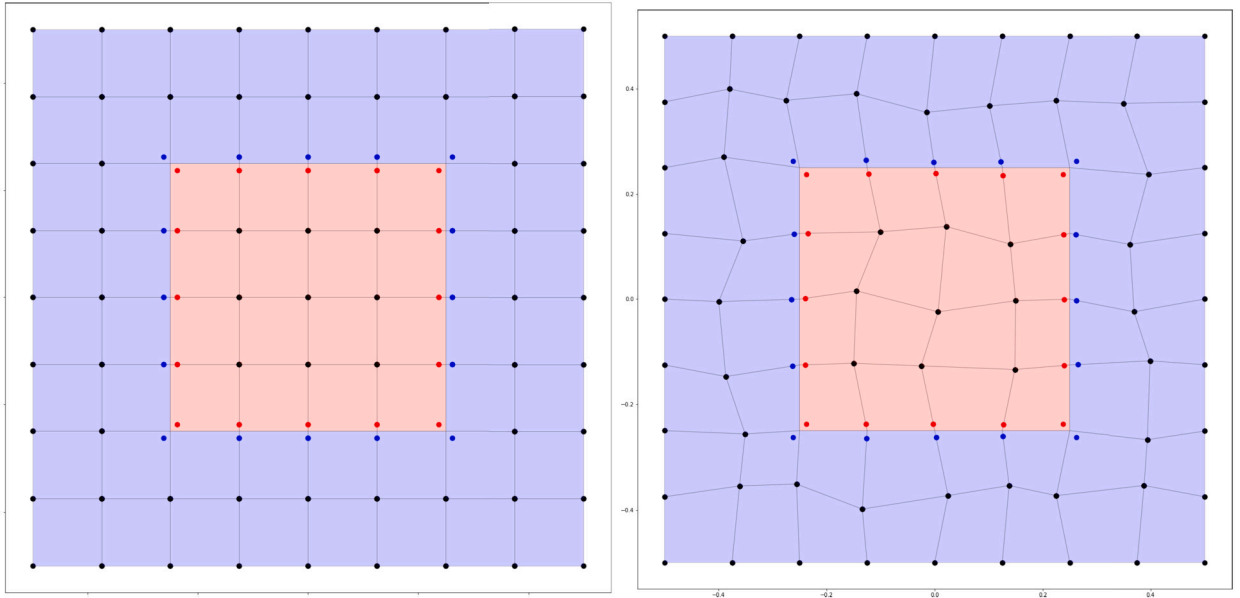


Fig. 4. Mesh sequences considered in the numerical test of Section 5.1.

The results reported in Fig. 5 and 6 show that the energy norm converges with order 1 (or slightly more), as predicted by Theorem 9 with  $r = 0$ . We additionally notice that the error is of comparable magnitude irrespectively of the value of  $\frac{\sigma_{\text{int}}}{\sigma_{\text{ext}}}$ , which confirms the robustness of the method with respect to the jumps of the diffusion coefficients discussed in Remark 10. As for the error in the  $L^2$ -like norm, convergence is close to second order, and its magnitude does not vary significantly with the ratio  $\frac{\sigma_{\text{int}}}{\sigma_{\text{ext}}}$ .

### 5.2. Circular interface

The second test introduces an additional difficulty, namely the fact that we deal with a curved interface. More specifically, in the square domain  $\Omega = [-1/2, 1/2]^2$ , we consider the circular interface  $\Gamma = \{(x, y) : x^2 + y^2 = R^2\}$  with  $R = 1/4$ . The convergence of the method is tested considering the following family of solutions  $u = (u_{\text{int}}, u_{\text{ext}})$ , represented in Fig. 7:

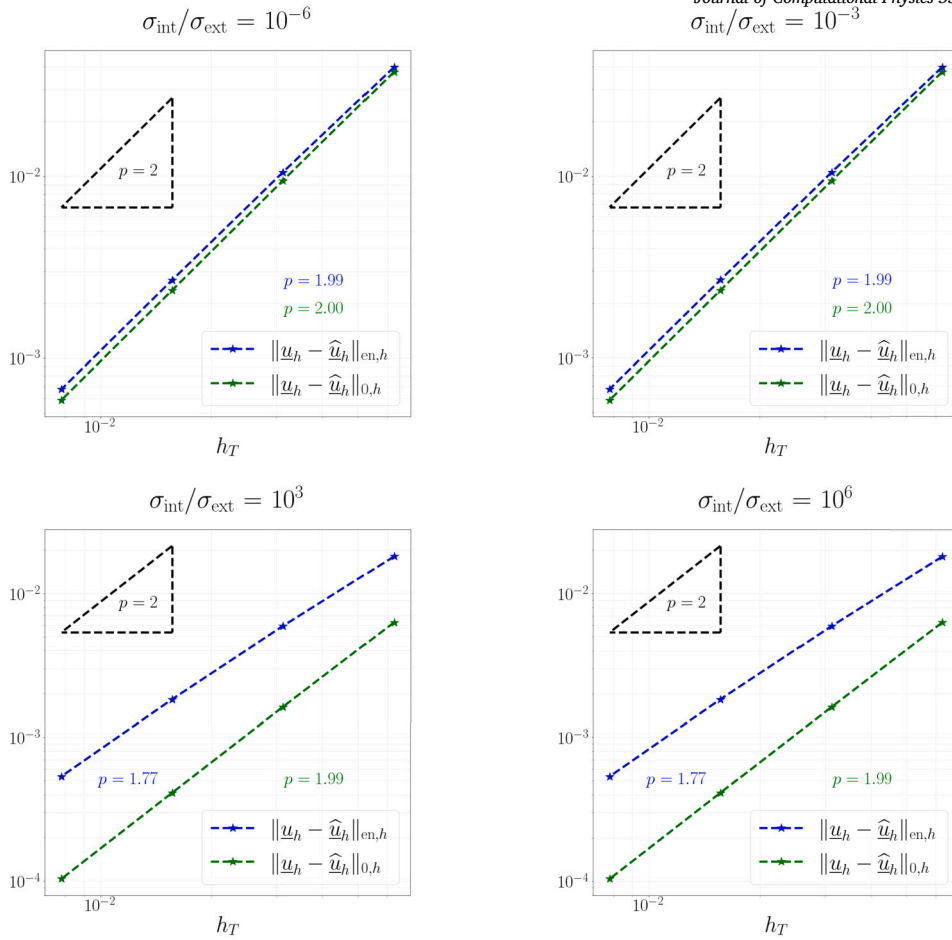


Fig. 5. Convergence for different values of  $\frac{\sigma_{\text{int}}}{\sigma_{\text{ext}}}$  over a mesh sequence of Cartesian orthogonal meshes, as described in Section 5.1. Error is normalized with respect to the norm of the reference solution.

$$u_{\text{int}} = \frac{2\sigma_{\text{ext}}}{\sigma_{\text{ext}} + \sigma_{\text{ext}}}x \quad u_{\text{ext}} = 1 + \left[ 1 + \left( \frac{\sigma_{\text{ext}} - \sigma_{\text{int}}}{\sigma_{\text{ext}} + \sigma_{\text{int}}} \right) \frac{R^2}{x^2 + y^2} \right]x. \quad (22)$$

We consider a sequence of unstructured triangular meshes of  $\Omega$  with mesh size halved at each refinement step and a family of polygonal discretizations of  $\Gamma$  with segment length divided by  $2^M$  at each refinement step (the integer  $M$  therefore represents the refinement ratio of the interface with respect to the background mesh: e.g., if  $M = 1$ , the background mesh and the interface are refined at the same rate). A fitted mesh is generated by splitting the elements of the original triangular mesh cut by the interface, as represented in Fig. 8. Please, notice that the number of interface edges of  $\mathcal{E}_{\Gamma,h}$  is greater than  $2^M$ , as interface edges that are intersected by edges of the simplicial mesh give place to at least 2 edges of the polygonal mesh originating from the cut. The test is then repeated with  $M = 4$  for different values of  $\sigma_{\text{int}}/\sigma_{\text{ext}}$  taken in  $\{10^{-6}, 10^{-3}, 10^3, 10^6\}$  to assess the convergence and robustness properties of the method. The results that are shown are obtained with  $\eta = 1$ ; see Fig. 10. As for the test of Section 5.1, slightly more than the theoretical convergence rate 1 is obtained for the energy norm. In order to explore the impact of the refinement ratio, in Fig. 9 we let  $\sigma_{\text{int}}/\sigma_{\text{ext}} = 10^{-1}$  and solve for several values of  $M$ . The results suggest that  $M = 2$  is sufficient to get the theoretical convergence rate 1, showing the ability of the method to capture curved interfaces without increasing the number of interface edges.

### 5.3. Generic interface

In the square domain  $\Omega = [-1/2, 1/2]^2$ , we consider a last test where the interface is obtained by deforming a circle. The additional difficulty comes from the fact that the curvature is no longer constant. To test the convergence of the method, we consider the family of polynomial solution (21) used for the case of a square interface depicted in Fig. 11. Keeping the refinement ratio  $M = 2$ , a convergence test showed in Fig. 12 is realized. The convergence rate over 1 confirms the theoretical prediction of Theorem 9.

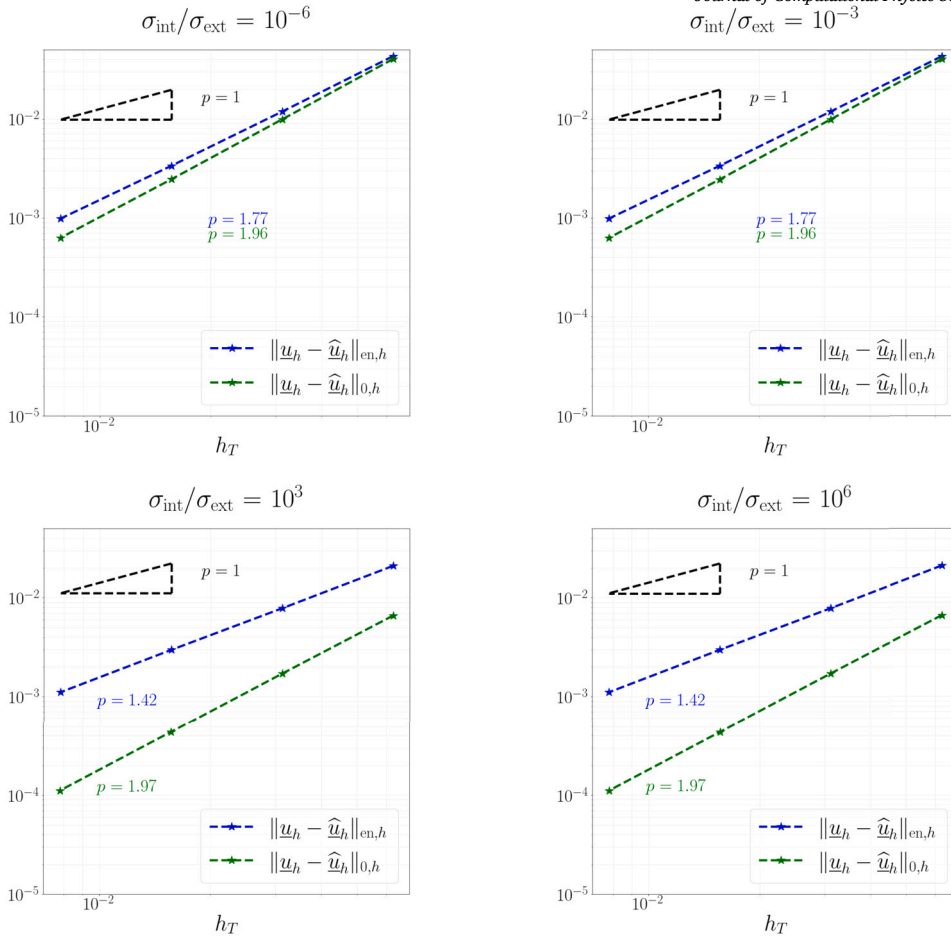


Fig. 6. Convergence for different values of  $\frac{\sigma_{\text{int}}}{\sigma_{\text{ext}}}$  over a mesh sequence of irregular quadrilaterals as described in Section 5.1. Error is normalized with respect to the norm of the reference solution.

## 6. Application to the Leaky Dielectric Model

In this section we discuss a version of problem (2) where the interface jump  $J_\Gamma$  is time dependent and obeys an evolution equation depending on the interface gradient of  $u = (u_{\text{int}}, u_{\text{ext}})$ .

### 6.1. Continuous setting

Given a final time  $t_f > 0$ , a source term  $f : (0, t_f] \rightarrow \mathbb{R}$ , and an initial potential jump  $J_\Gamma^0$ , we consider the problem of finding the time-dependent potential  $u = (u_{\text{int}}, u_{\text{ext}})$  with  $u_\bullet : \Omega_\bullet \times (0, t_f] \rightarrow \mathbb{R}$ ,  $\bullet \in \{\text{int}, \text{ext}\}$  and the interface jump  $J_\Gamma : \Gamma \times [0, t_f] \rightarrow \mathbb{R}$  such that

$$-\nabla \cdot (\sigma_\bullet \nabla u_\bullet) = f \quad \text{in } \Omega_\bullet \times (0, t_f], \bullet \in \{\text{int}, \text{ext}\}, \quad (23a)$$

$$[u]_\Gamma = J_\Gamma \quad \text{on } \Gamma \times (0, t_f], \quad (23b)$$

$$[\sigma \nabla u]_\Gamma \cdot n_\Gamma = 0 \quad \text{on } \Gamma \times (0, t_f], \quad (23c)$$

$$u_{\text{ext}} = 0 \quad \text{on } \partial\Omega \times (0, t_f] \quad (23d)$$

$$C \partial_t J_\Gamma = \sigma_\bullet \nabla u_\bullet \cdot n_\Gamma \quad \text{on } \Gamma \times (0, t_f], \bullet \in \{\text{int}, \text{ext}\} \quad (23e)$$

$$J_\Gamma(\cdot, 0) = J_\Gamma^0 \quad \text{on } \Gamma, \quad (23f)$$

with  $C > 0$ . Problem (23) models a situation where two media with electric conductivity respectively equal to  $\sigma_{\text{int}}$  and  $\sigma_{\text{ext}}$  occupy the regions  $\Omega_{\text{int}}$  and  $\Omega_{\text{ext}}$ . The interface  $\Gamma$  between the two media is characterized by a capacitance  $C$ . The variation rate of the charge in the bulk is  $f$  and the interface supports no surface charge. The region  $\Omega_\bullet$  with  $\bullet \in \{\text{int}, \text{ext}\}$  is characterized by an electrostatic potential  $u_\bullet$  to determine. The potential is discontinuous at the interface, with a jump  $J_\Gamma$  to determine, and vanishes on the boundary of  $\Omega$ .

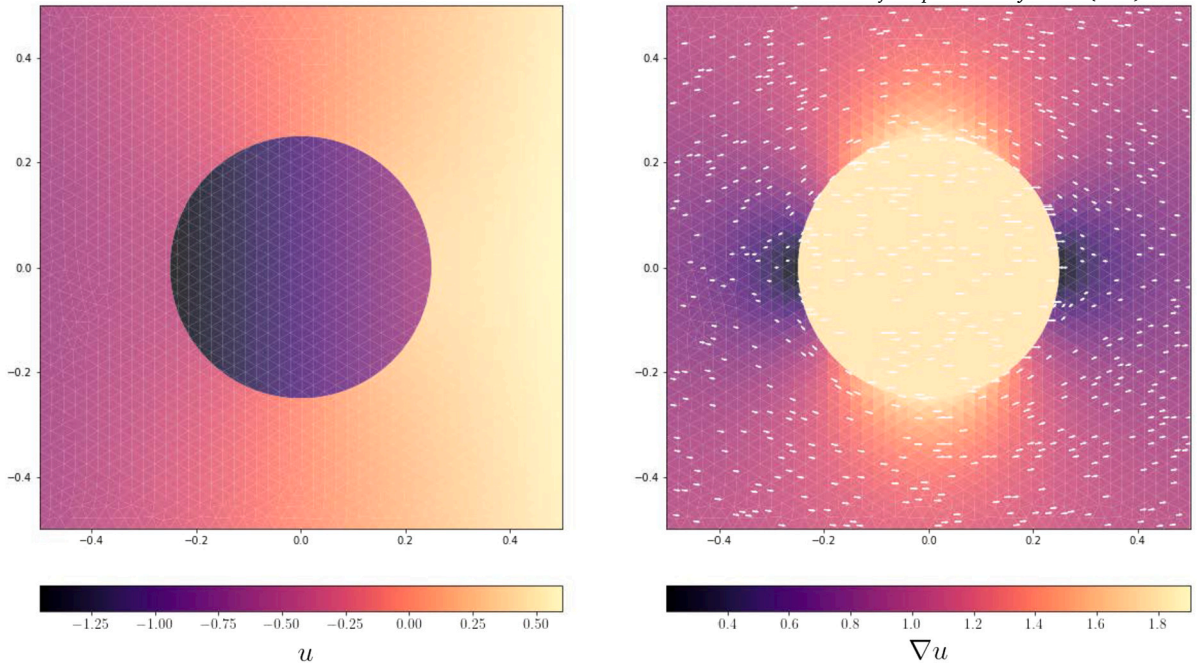


Fig. 7. The exact solution (22) considered in Section 5.2 and its gradient with  $\frac{\sigma_{\text{int}}}{\sigma_{\text{ext}}} = 10^{-1}$ .

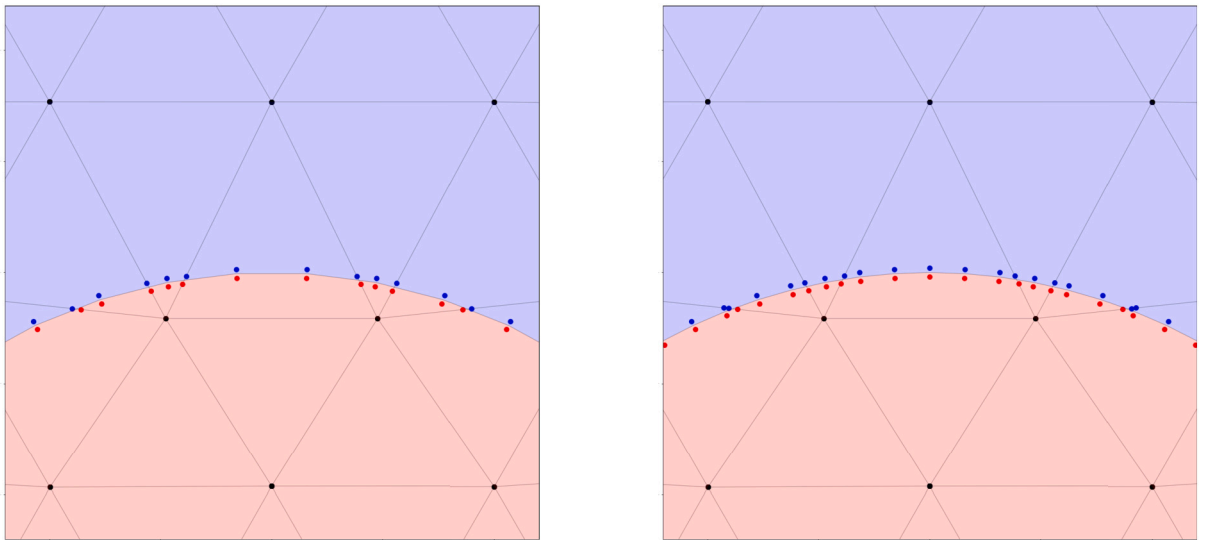


Fig. 8. Mesh family used in the example from Section 5.2. The detail shows new elements generated by cutting a triangular mesh with a polygonal discretization of the interface. Spots represent the distribution of degrees of freedom. The same background triangular mesh can be cut using different refinement levels for the interface. The accuracy of discretization of  $\Gamma$  is therefore arbitrary.

### 6.2. Discrete problem

To adapt the scheme (15) to problem (23), it is necessary to introduce a time stepping scheme and a suitable discrete space to describe the new variable  $J_\Gamma$ . For the sake of simplicity, we describe the adaption in the case of  $k = 0$ . Consider  $N \geq 1$  time steps with duration  $\tau = t/N$ . For any time-dependent variable  $w$ , we introduce the set of time-independent variables  $\{w^n\}_{n \leq N}$  such that  $w^n(x) = w(x, n\tau)$ . An explicit Euler scheme is adopted to replace (23e) with:

$$\frac{C}{\tau} (J_\Gamma^{n+1} - J_\Gamma^n) = \sigma_{\text{int}} \nabla u_{\text{int}}^n \cdot n_\Gamma = \sigma_{\text{ext}} \nabla u_{\text{ext}}^n \cdot n_\Gamma.$$

The equation is integrated along  $\Gamma$  after multiplying by a test function  $Q_\Gamma^n : \Gamma \rightarrow \mathbb{R}$ :

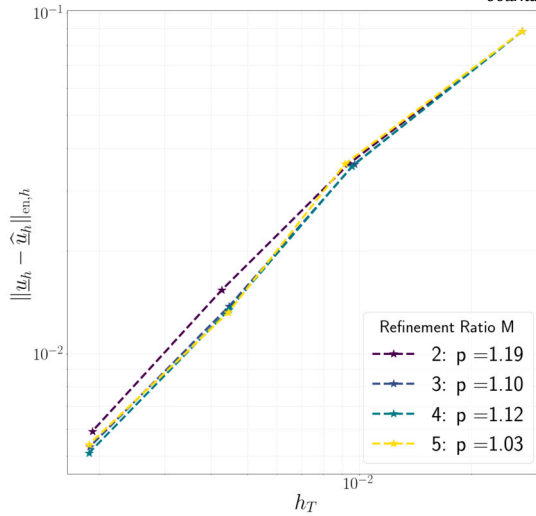


Fig. 9. Convergence test described in Section 5.2, keeping  $\sigma_{\text{int}}/\sigma_{\text{ext}} = 0.1$  and varying the refinement ratio  $M$ .

$$\frac{C}{\tau} \left( \int_{\Gamma} J_{\Gamma}^{n+1} Q_{\Gamma}^n - \int_{\Gamma} J_{\Gamma}^n Q_{\Gamma}^n \right) = \int_{\Gamma} (\sigma_{\text{int}} \nabla u_{\text{int}}^n \cdot n_{\Gamma}) Q_{\Gamma}^n = \int_{\Gamma} (\sigma_{\text{ext}} \nabla u_{\text{ext}}^n \cdot n_{\Gamma}) Q_{\Gamma}^n.$$

Consider the collection of interface vertices  $\mathcal{V}_{\Gamma,h}$  and introduce the space of interface variables:

$$\underline{Z}_{\Gamma,h} := \left\{ p_{\Gamma,h} = (p_V)_{V \in \mathcal{V}_{\Gamma,h}} : p_V \in \mathbb{R} \quad \forall V \in \mathcal{V}_{\Gamma,h} \right\}.$$

Given  $p_{\Gamma,h} \in \underline{Z}_{\Gamma,h}$  and  $E \in \mathcal{E}_{\Gamma,h}$ , define  $p_E \in \mathcal{P}^1(E)$  as the unique affine function that takes the value  $p_V$  at every endpoint  $V$  of  $E$ . Equip  $\underline{Z}_{\Gamma,h}$  with the following norm:

$$\|p_{\Gamma,h}\|_{0,\Gamma,h}^2 := \sum_{E \in \mathcal{E}_{\Gamma,h}} \|p_E\|_E^2.$$

We set  $\underline{J}_{\Gamma,h}^0 := (J_{\Gamma}^0(x_V))_{V \in \mathcal{V}_{\Gamma,h}}$ , with  $x_V$  denoting the coordinate vector of the vertex  $V$  and, for  $n = 0, \dots, N - 1$ , we advance in time solving the following problem: Find  $\underline{J}_{\Gamma,h}^{n+1} \in \underline{Z}_{\Gamma,h}$  such that

$$\frac{C}{\tau} \left( \sum_{E \in \mathcal{E}_{\Gamma,h}} \int_E J_E^{n+1} Q_E^n - \int_E J_E^n Q_E^n \right) = \sum_{E \in \mathcal{E}_{\Gamma,h}} \int_E \{\sigma G_T \underline{u}_T\}_{\lambda,E} \cdot n_{\Gamma} Q_E \quad \forall \underline{Q}_{\Gamma,h}^n \in \underline{Z}_{\Gamma,h}. \tag{24}$$

Given  $\underline{J}_{\Gamma,h}^n \in \underline{Z}_{\Gamma,h}^k$ , denote by  $\mathcal{M}_h : \underline{Z}_{\Gamma,h}^k \rightarrow \underline{V}_h^0$  the operator that associates to a jump  $\underline{J}_{\Gamma}^n$  the solution  $\underline{u}_h$  of the stationary problem (15). Likewise, call  $\mathcal{N}_h : \underline{V}_h^0 \times \underline{Z}_{\Gamma,h} \rightarrow \underline{Z}_{\Gamma,h}$  the operator that associates to a potential  $\underline{u}_h$  and a jump  $\underline{J}_{\Gamma,h}^n$  the jump  $\underline{J}_{\Gamma,h}^{n+1}$  solution to problem (24). Then, the time advancement algorithm for the case of an evolving jump reads: Given  $\underline{J}_{\Gamma,h}^0$ , for  $n = 0, \dots, N - 1$ , set, in this order,

$$\begin{aligned} \underline{u}_h^n &= \mathcal{M}_h(\underline{J}_{\Gamma}^n), \\ \underline{J}_{\Gamma,h}^{n+1} &= \mathcal{N}_h(\underline{u}_h^n, \underline{J}_{\Gamma,h}^n). \end{aligned}$$

### 6.3. Numerical tests

To numerically assess the performance method, we consider a test case with  $f = 0$ ,  $\Phi_{\Gamma} = 0$ ,  $J_{\Gamma}^0 = 0$ . This set of conditions is encountered in the description of the electric potential in the context of the Leaky Dielectric Model, and represents a situation where neither the bulk nor the surface support electric charge. Consider a circular interface of radius  $R > 0$  immersed in a uniform far field  $\epsilon \in \mathbb{R}^2$ , such that  $\lim_{\|x\| \rightarrow \infty} \nabla u = \epsilon$ , with  $\|\cdot\|$  denoting the Euclidean norm in  $\mathbb{R}^2$ . With  $\bullet \in \{\text{int}, \text{ext}\}$ , and centering the reference system at the origin of the circle, the solution reads:

$$\hat{u}_{\bullet}(x, t) = \exp\left(-\frac{t}{t_c}\right) (u_{\bullet}^0(x) - u_{\bullet}^{\infty}(x)) + u_{\bullet}^{\infty}(x), \tag{25}$$

with

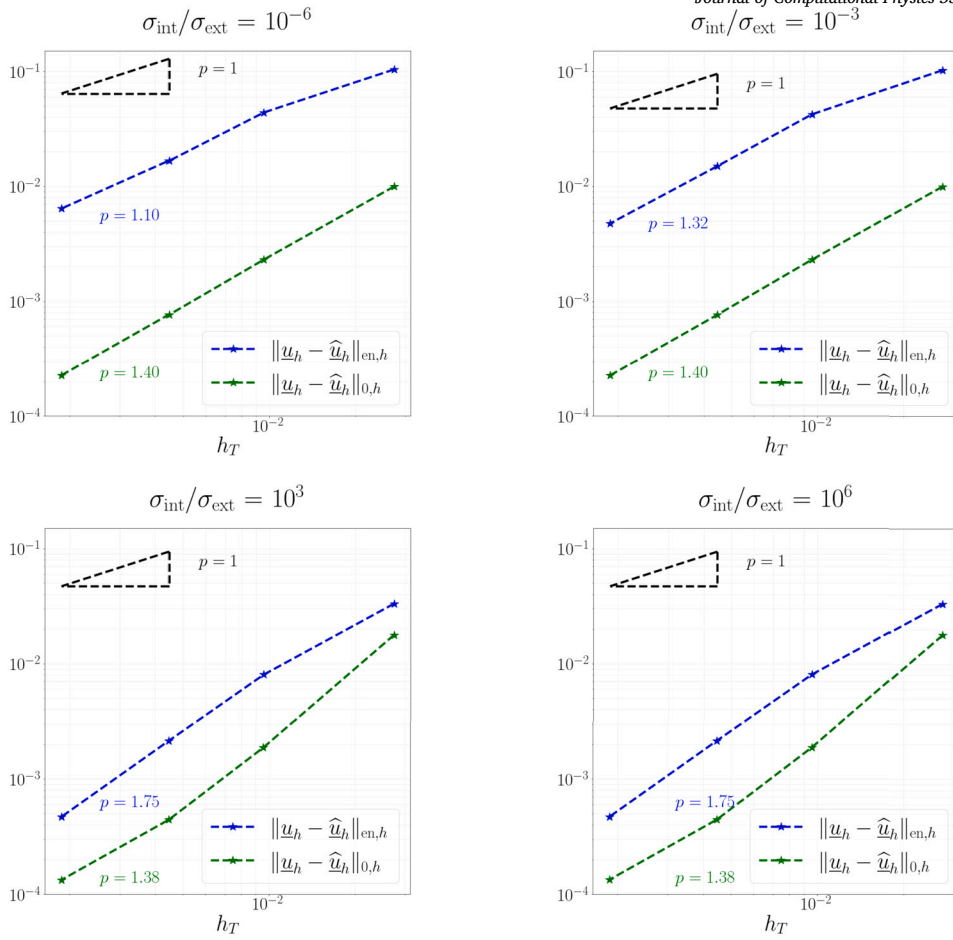


Fig. 10. Convergence test from Section 5.2. With refinement ratio  $M = 4$  the test is repeated for several values of  $\frac{\sigma_{int}}{\sigma_{ext}}$ . Error is normalized with respect to the norm of the reference solution.

$$\begin{aligned}
 u_{int}^0 &= \left( \frac{2\sigma_{ext}}{\sigma_{ext} + \sigma_{int}} \right) x \cdot \epsilon & u_{ext}^0 &= \left[ 1 + \left( \frac{\sigma_{ext} - \sigma_{int}}{\sigma_{ext} + \sigma_{int}} \right) \frac{R^2}{\|x\|^2} \right] x \cdot \epsilon \\
 u_{int}^\infty &= 0 & u_{ext}^\infty &= \left( 1 + \frac{R^2}{\|x\|^2} \right) x \cdot \epsilon
 \end{aligned}$$

and  $t_c = CR \left( \frac{1}{\sigma_{int}} + \frac{1}{\sigma_{ext}} \right)$  (see Fig. 13). The system evolves from an initial condition with no potential jump at the interface to a condition of electrostatic equilibrium, where the current flow through the interface  $\nabla u \cdot n_\Gamma$  with  $\bullet \in \{\text{int}, \text{ext}\}$  vanishes from either side as well as the internal electric field.

To monitor the convergence of the scheme, we consider a mesh sequence realized with the same family of triangular background meshes of Section 5.2. The interface is refined with a refinement ratio  $M = 2$ , and a sequence of time steps decreasing by a factor 4 is considered. The results that are shown are obtained with  $\eta = 1$ . The profile of the error for both the potential  $u = (u_{int}, u_{ext})$  and the jump  $J_\Gamma$  is displayed in Fig. 14. Results show that the  $L^2$ -temporal norm of the energy error decreases with an order slightly lower than 1. An convergence slightly above 0.5 is observed for the time-space  $L^2$ -norm of the interface jump.

## 7. Proofs of the main results

This section collects the proofs of Lemma 7 and Theorem 9.

### 7.1. Proof of Lemma 7

**Lemma 12** (Estimate of the consistency interface term). *Then, for all  $(\underline{w}_h, \underline{v}_h) \in \underline{V}_h^k \times \underline{V}_h^k$  and any real number  $\epsilon > 0$ , it holds, with  $N_\partial$  as in Lemma 7,*

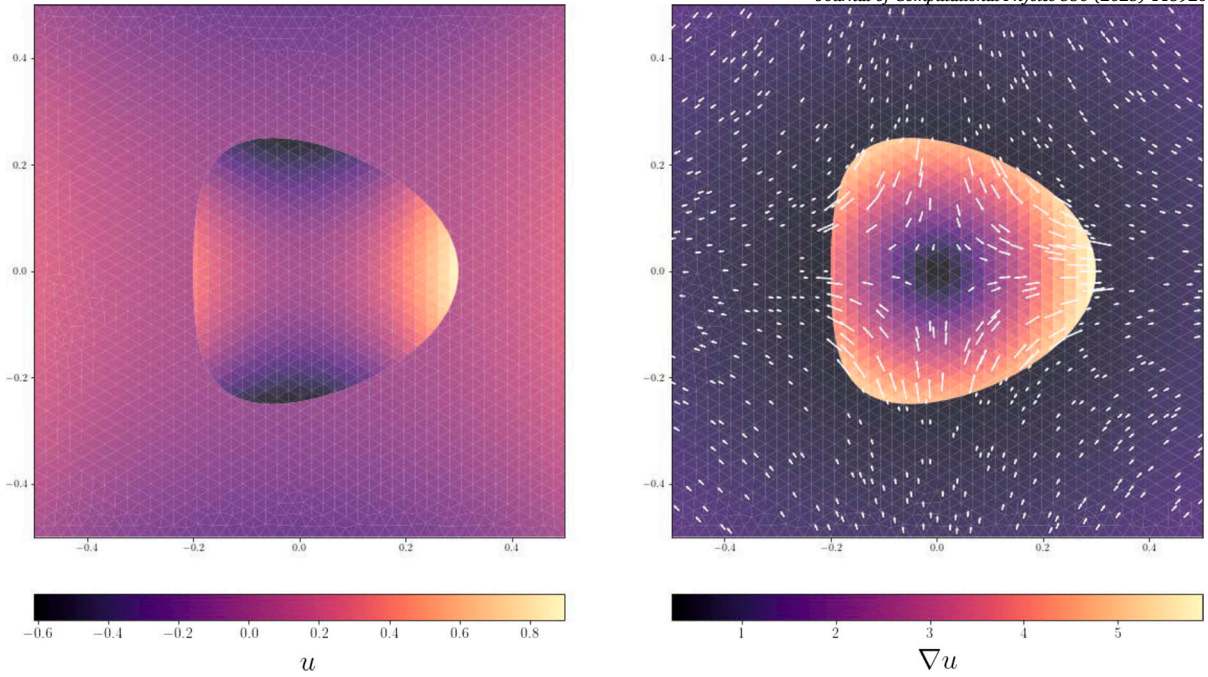


Fig. 11. The exact solution (21) considered in Section 5.3 and its gradient with  $\frac{\sigma_{\text{int}}}{\sigma_{\text{ext}}} = 10^{-1}$ .

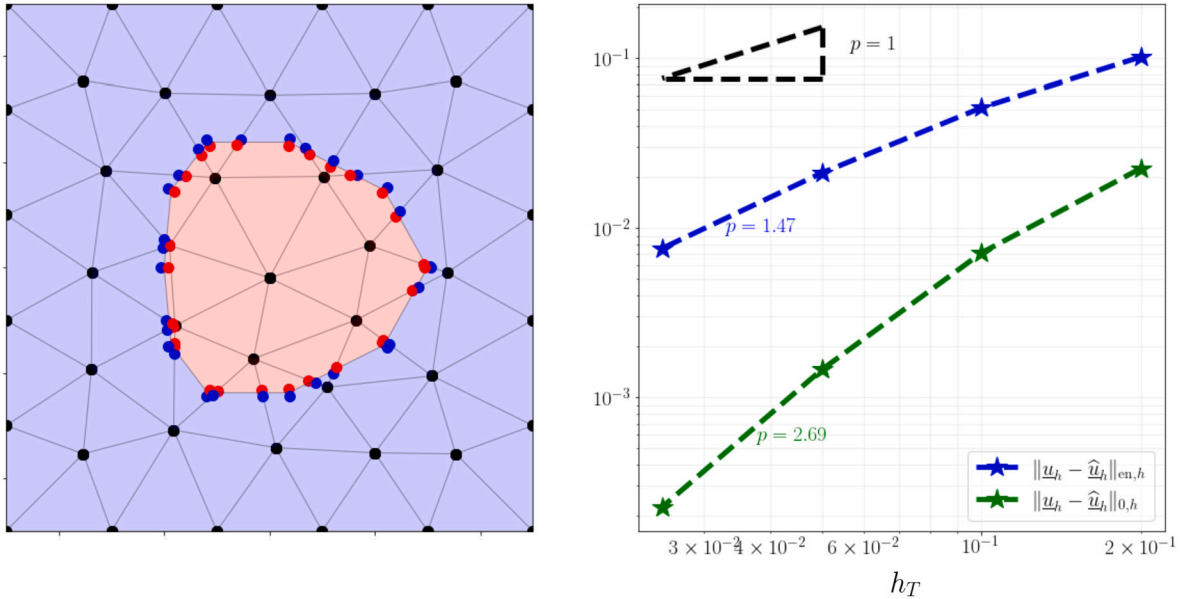
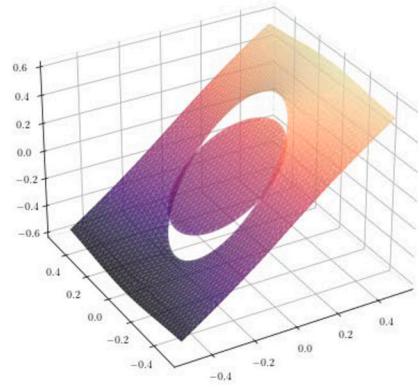
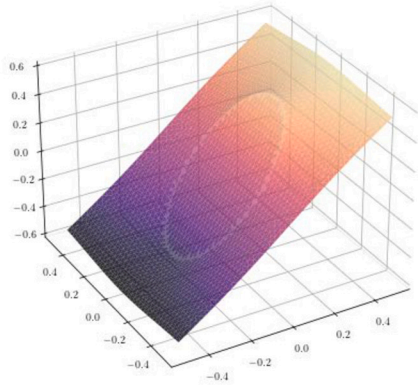


Fig. 12. Convergence test for the case of a generic interface of Section 5.3. On the left, a member of the mesh sequence. The red area represents  $\Omega_{\text{int}}$  and the blue one  $\Omega_{\text{ext}}$ . Dots represent the distribution of degrees of freedom for the first element of the mesh sequence. On nodes belonging to  $\Gamma$  they are doubled. On the right,  $p$  indicates the estimated convergence order. (For interpretation of the colors in the figure(s), the reader is referred to the web version of this article.)

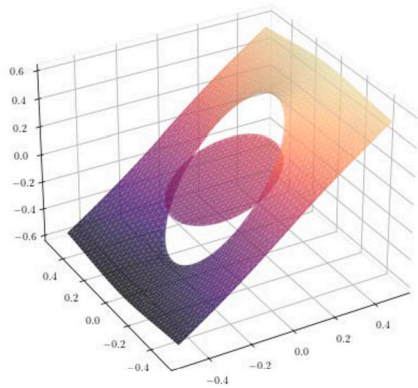
$$\sum_{E \in \mathcal{E}_{\Gamma,h}} \int \{ \sigma G_h^k \underline{w}_h \}_{\lambda,E} \cdot n_E [\underline{v}_h]_E \leq \epsilon \| \sigma^{1/2} G_h^k \underline{w}_h \|_{L^2(\Omega)^2}^2 + \frac{C_{\text{tr}}^2 N_d}{4\epsilon} |\underline{v}_h|_{1,h}^2. \tag{26}$$

**Proof.** Let  $E \in \mathcal{E}_{\Gamma,h}$ . Using a  $(2, \infty, 2)$ -Hölder inequality, we can write

t = 0



t = 1.0



t = 1.5

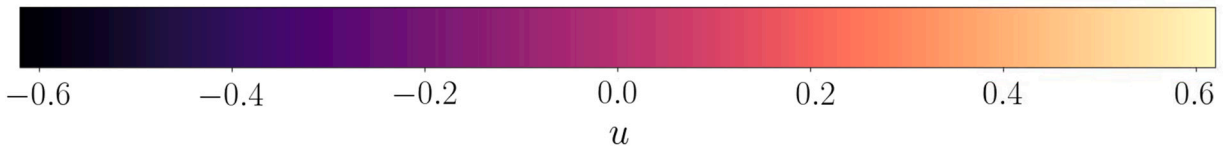
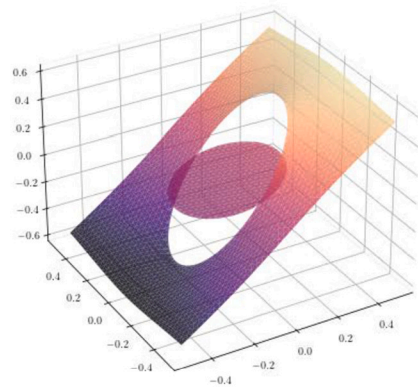


Fig. 13. Solution (25) presented in Section 6. Test performed with  $R = 1/4$ ,  $\|\epsilon\| = 1$ ,  $\sigma_{\text{int}}/\sigma_{\text{ext}} = 10^{-1}$ , and  $C$  set such that  $t_c = 1$ .

$$\begin{aligned} & \int_E \{\sigma G_h^k \underline{w}_h\}_{\lambda, E} \cdot n_E [\underline{v}_h]_E \\ & \leq \| \{\sigma G_h^k \underline{w}_h\}_{\lambda, E} \|_{L^2(E)^2} \| n_E \|_{L^\infty(E)^2} \| [\underline{v}_h]_E \|_{L^2(E)} \\ & \stackrel{(11)}{\leq} \alpha^{-1/2} \left( \lambda_{\text{int}} \sigma_{\text{int}}^{1/2} \| \sigma_{\text{int}}^{1/2} G_{T_{\text{int}}}^k \underline{w}_{T_{\text{int}}} \|_{L^2(E)^2} + \lambda_{\text{ext}} \sigma_{\text{ext}}^{1/2} \| \sigma_{\text{ext}}^{1/2} G_{T_{\text{ext}}}^k \underline{w}_{T_{\text{ext}}} \|_{L^2(E)^2} \right) \alpha^{1/2} \| [\underline{v}_h]_E \|_{L^2(E)}, \end{aligned}$$

where, in the second equality, we have additionally used the fact that  $\|n_E\|_{L^\infty(E)^2} \leq 1$ . Noticing that, by definition (10) of  $\lambda_\bullet$  and (13) of  $\alpha$ , and since  $\lambda_\bullet < 1$ ,

$$\frac{\lambda_\bullet^2 \sigma_\bullet}{\alpha} < \frac{1}{2} \quad \bullet \in \{\text{int}, \text{ext}\}, \tag{27}$$

we can go on writing

$$\int_E \{\sigma G_h^k \underline{w}_h\}_{\lambda, E} \cdot n_E [\underline{v}_h]_E$$

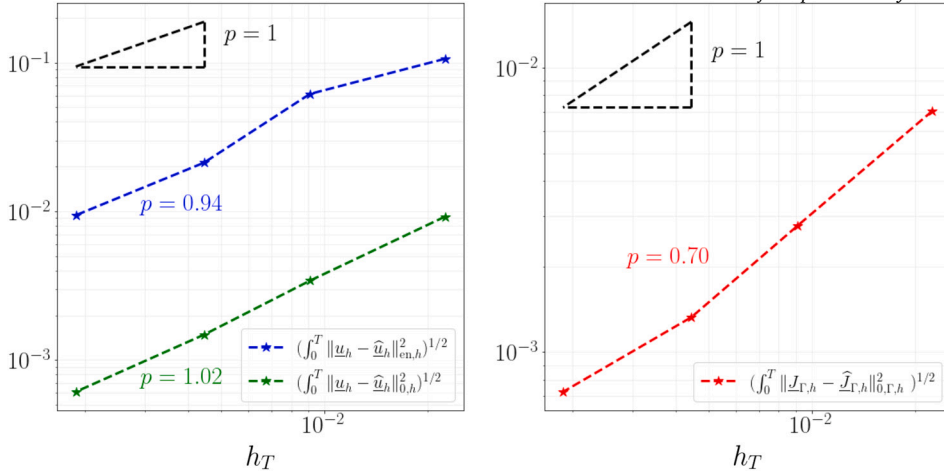


Fig. 14. Convergence test for the time-dependent scheme used to reproduce Solution (25) presented in Section 6. The simulation is run with  $t_f = 2t_c = 2$ .

$$\begin{aligned} &\leq \frac{1}{\sqrt{2}} \left( \|\sigma_{\text{int}}^{1/2} G_{T_{\text{int}}}^k \underline{w}_{T_{\text{int}}}\|_{L^2(E)^2} + \|\sigma_{\text{ext}}^{1/2} G_{T_{\text{ext}}}^k \underline{w}_{T_{\text{ext}}}\|_{L^2(E)^2} \right) \alpha^{1/2} \|\llbracket \underline{v}_h \rrbracket_E\|_{L^2(E)} \\ &\stackrel{(18), (17)}{\leq} \frac{C_{\text{tr}}}{\sqrt{2}} \left( \|\sigma_{\text{int}}^{1/2} G_{T_{\text{int}}}^k \underline{w}_{T_{\text{int}}}\|_{L^2(T_{\text{int}})^2} + \|\sigma_{\text{ext}}^{1/2} G_{T_{\text{ext}}}^k \underline{w}_{T_{\text{ext}}}\|_{L^2(T_{\text{ext}})^2} \right) \left( \frac{\alpha}{h_E} \right)^{1/2} \|\llbracket \underline{v}_h \rrbracket_E\|_{L^2(E)}. \end{aligned}$$

Summing the above inequality over  $E \in \mathcal{E}_{\Gamma,h}$ , using a Cauchy–Schwarz inequality along with the fact that  $(a + b)^2 \leq 2(a^2 + b^2)$ , and recalling the definition (17) of  $|\cdot|_{J,h}$ , we obtain

$$\begin{aligned} &\sum_{E \in \mathcal{E}_{\Gamma,h}} \int_E \{ \sigma G_h^k \underline{w}_h \}_{\lambda,E} \cdot n_E \llbracket \underline{v}_h \rrbracket_E \\ &\leq C_{\text{tr}} \left[ \sum_{E \in \mathcal{E}_{\Gamma,h}} \left( \|\sigma_{\text{int}}^{1/2} G_{T_{\text{int}}}^k \underline{w}_{T_{\text{int}}}\|_{L^2(T_{\text{int}})^2}^2 + \|\sigma_{\text{ext}}^{1/2} G_{T_{\text{ext}}}^k \underline{w}_{T_{\text{ext}}}\|_{L^2(T_{\text{ext}})^2}^2 \right) \right]^{1/2} |\underline{v}_h|_{J,h} \\ &\leq C_{\text{tr}} N_\partial^{1/2} \|\sigma^{1/2} G_h^k \underline{w}_h\|_{L^2(\Omega)^2} |\underline{v}_h|_{J,h} \\ &\leq \epsilon \|\sigma^{1/2} G_h^k \underline{w}_h\|_{L^2(\Omega)^2}^2 + \frac{C_{\text{tr}}^2 N_\partial}{4\epsilon} |\underline{v}_h|_{J,h}^2, \end{aligned}$$

the conclusion being a consequence of the generalized Young’s inequality.  $\square$

**Proof of Lemma 7.** Recalling the expression (12) of  $a_h$  and using (26), we obtain, for all  $\underline{v}_h \in \underline{V}_{h,0}^k$ ,

$$a_h(\underline{v}_h, \underline{v}_h) \geq (1 - \epsilon) \|\sigma^{1/2} G_h^k \underline{v}_h\|_{L^2(\Omega)^2}^2 + \sum_{T \in \mathcal{T}_h} \frac{\sigma_T}{h_T} \sum_{E \in \mathcal{E}_T} \|p_T^{k+1} \underline{v}_T - v_{TE}\|_{L^2(E)^2}^2 + \left( \eta - \frac{C_{\text{tr}}^2 N_\partial}{4\epsilon} \right) |\underline{v}_h|_{J,h}^2,$$

from which the conclusion readily follows recalling the definition (16) of the energy norm.  $\square$

### 7.2. Proof of Theorem 9

**Lemma 13 (Estimate of the consistency error).** Assume  $u \in C^0(\overline{\Omega}_{\text{int}}) \times C^0(\overline{\Omega}_{\text{ext}})$  and define the consistency error linear form  $\mathcal{E}_h : \underline{V}_{h,0}^k \rightarrow \mathbb{R}$  such that, for all  $\underline{v}_h \in \underline{V}_{h,0}^k$ ,

$$\mathcal{E}_h(\underline{v}_h) := \ell_h(\underline{v}_h) - a_h(\underline{I}_h^k u, \underline{v}_h).$$

Then, provided that  $u \in H^{r+2}(\mathcal{T}_h^{\text{int}}) \times H^{r+2}(\mathcal{T}_h^{\text{ext}})$  for some  $r \in \{0, \dots, k\}$ , it holds

$$\sup_{\underline{v}_h \in \underline{V}_{h,0}^k \setminus \{0\}} \frac{\mathcal{E}_h(\underline{v}_h)}{\|\underline{v}_h\|_{\text{en},h}} \lesssim \bar{\sigma} h^{r+1} |u|_{H^{r+2}(\mathcal{T}_h)}, \tag{28}$$

where the hidden constant depends only on the domain, the stability constant  $C_{\text{stab}}$  in (20), the polynomial degree  $k$ , and the mesh regularity parameter (but is independent of both the meshsize and  $\sigma$ ).

**Proof.** Let  $\underline{v}_h \in \underline{V}_{h,0}^k$ . We reformulate the components of the consistency error  $\mathcal{E}_h(\underline{v}_h)$  in order to make them comparable. Throughout the proof we let, for the sake of brevity,  $\hat{\underline{u}}_h := \underline{I}_h^k u$ .  
**1. Reformulation of  $\ell_h(\underline{v}_h)$ .** Recalling (2a),  $f = -\nabla \cdot (\sigma \cdot \nabla u)$  almost everywhere in  $\Omega$ ,  $\bullet \in \{\text{int}, \text{ext}\}$ . We can therefore write for the first term in the right-hand side of (14):

$$\begin{aligned} \sum_{T \in \mathcal{T}_h} \int_T f p_T^{k+1} \underline{v}_T &= - \sum_{T \in \mathcal{T}_h} \int_T \nabla \cdot (\sigma_T \nabla u) p_T^{k+1} \underline{v}_T \\ &= \sum_{T \in \mathcal{T}_h} \int_T \sigma_T \nabla u \cdot \nabla p_T^{k+1} \underline{v}_T - \sum_{T \in \mathcal{T}_h} \sum_{E \in \mathcal{E}_T} \omega_{TE} \int_E (\sigma_T \nabla u \cdot n_E) p_T^{k+1} \underline{v}_T \\ &= \sum_{T \in \mathcal{T}_h} \int_T \sigma_T \nabla u \cdot \nabla p_T^{k+1} \underline{v}_T - \sum_{T \in \mathcal{T}_h} \sum_{E \in \mathcal{E}_T} \omega_{TE} \int_E (\sigma_T \nabla u \cdot n_E) (p_T^{k+1} \underline{v}_T - v_{TE}) \\ &\quad - \underbrace{\sum_{T \in \mathcal{T}_h} \sum_{E \in \mathcal{E}_T} \omega_{TE} \int_E (\sigma_T \nabla u \cdot n_E) v_{TE}}_{\mathfrak{I}}, \end{aligned} \tag{29}$$

where we have used an integration by parts inside each element in the second equality and inserted  $\pm v_{TE}$  into the boundary term to conclude. Let us focus on the last term. Rearranging the sums, we have

$$\begin{aligned} \mathfrak{I} &= \sum_{E \in \mathcal{E}_h} \sum_{T \in \mathcal{T}_E} \omega_{TE} \int_E (\sigma_T \nabla u \cdot n_E) v_{TE} \\ &= \sum_{E \in \mathcal{E}_{\Gamma,h}} \int_E \left[ (\sigma_{T_{\text{int}}} \nabla u_{\text{int}} \cdot n_E) v_{T_{\text{int}} E} - (\sigma_{T_{\text{ext}}} \nabla u_{\text{ext}} \cdot n_E) v_{T_{\text{ext}} E} \right], \end{aligned}$$

where we have used the fact that both  $v_{TE}$  and the normal trace of  $\sigma \nabla u$  are single-valued on mesh edges internal to each subdomain along with the fact that  $v_{TE} = 0$  on edges contained in  $\partial \Omega$  in the second equality. We next notice that, given four real numbers  $a_1$ ,  $a_2$ ,  $b_1$ , and  $b_2$ , since  $\lambda_{\text{int}} + \lambda_{\text{ext}} = 1$  (cf. (10)),

$$a_1 b_1 - a_2 b_2 = (\lambda_{\text{int}} a_1 + \lambda_{\text{ext}} a_2)(b_1 - b_2) + (a_1 - a_2)(\lambda_{\text{ext}} b_1 + \lambda_{\text{int}} b_2).$$

Applying this formula with  $(a_1, a_2, b_1, b_2) = (\sigma_{\text{int}} \nabla u_{\text{int}} \cdot n_E, \sigma_{\text{ext}} \nabla u_{\text{ext}} \cdot n_E, v_{T_{\text{int}} E}, v_{T_{\text{ext}} E})$ , recalling the definitions of the interface trace operators of Section 4.3, and using the fact that, by (2c),  $[\sigma \nabla u]_E \cdot n_E = \Phi_\Gamma$  almost everywhere on  $\Gamma$ , we infer that

$$\mathfrak{I} = \sum_{E \in \mathcal{E}_{\Gamma,h}} \int_E \{ \sigma \nabla u \}_{\lambda,E} \cdot n_E [\underline{v}_h]_E + \sum_{E \in \mathcal{E}_{\Gamma,h}} \int_E \Phi_\Gamma \{ \underline{v}_h \}_{\lambda,E}.$$

Plugging this expression into (29) and substituting into the expression (14) of  $\ell_h$ , we arrive at

$$\begin{aligned} \ell_h(\underline{v}_h) &= \sum_{T \in \mathcal{T}_h} \int_T \sigma_T \nabla u \cdot \nabla p_T^{k+1} \underline{v}_T - \sum_{T \in \mathcal{T}_h} \sum_{E \in \mathcal{E}_T} \omega_{TE} \int_E (\sigma_T \nabla u \cdot n_E) (p_T^{k+1} \underline{v}_T - v_{TE}) \\ &\quad - \sum_{E \in \mathcal{E}_{\Gamma,h}} \int_E \{ \sigma \nabla u \}_{\lambda,E} \cdot n_E [\underline{v}_h]_E + \eta \sum_{E \in \mathcal{E}_{\Gamma,h}} \frac{\alpha}{h_E} \int_E J_\Gamma [\underline{v}_h]_E. \end{aligned} \tag{30}$$

**2. Reformulation of  $a_h(\hat{\underline{u}}_h, \underline{v}_h)$ .** Let  $T \in \mathcal{T}_h$ . Writing (4) for  $\tau = \sigma_T G_T^k \hat{\underline{u}}_T$  and rearranging, we obtain

$$\int_T \sigma_T G_T^k \hat{\underline{u}}_T \cdot G_T^k \underline{v}_T = \int_T \sigma_T G_T^k \hat{\underline{u}}_T \cdot \nabla p_T^{k+1} \underline{v}_T - \sum_{E \in \mathcal{E}_T} \omega_{TE} \int_E (\sigma_T G_T^k \hat{\underline{u}}_T \cdot n_E) (p_T^{k+1} \underline{v}_T - v_{TE}).$$

Substituting this expression in the definition (12) of  $a_h$  written for  $\underline{w}_h = \hat{\underline{u}}_h$ , we obtain

$$\begin{aligned} a_h(\hat{\underline{u}}_h, \underline{v}_h) &:= \sum_{T \in \mathcal{T}_h} \int_T \sigma_T G_T^k \hat{\underline{u}}_T \cdot \nabla p_T^{k+1} \underline{v}_T - \sum_{T \in \mathcal{T}_h} \sum_{E \in \mathcal{E}_T} \omega_{TE} \int_E (\sigma_T G_T^k \hat{\underline{u}}_T \cdot n_E) (p_T^{k+1} \underline{v}_T - v_{TE}) \\ &\quad + \sum_{T \in \mathcal{T}_h} \frac{\sigma_T}{h_T} \sum_{E \in \mathcal{E}_T} \int_E (p_T^{k+1} \hat{\underline{u}}_T - \hat{\underline{u}}_{TE}) (p_T^{k+1} \underline{v}_T - v_{TE}) \\ &\quad - \sum_{E \in \mathcal{E}_{\Gamma,h}} \int_E \{ \sigma G_h^k \hat{\underline{u}}_h \}_{\lambda,E} \cdot n_E [\underline{v}_h]_E + \eta \sum_{E \in \mathcal{E}_{\Gamma,h}} \frac{\alpha}{h_E} \int_E [\hat{\underline{u}}_h]_E [\underline{v}_h]_E. \end{aligned} \tag{31}$$

**3. Estimate of the consistency error.** Subtracting (31) from (30), we arrive at the following decomposition of the consistency error:

$$\mathcal{E}_h(\underline{v}_h) = \mathfrak{T}_1 + \dots + \mathfrak{T}_5$$

with

$$\begin{aligned} \mathfrak{T}_1 &:= \sum_{T \in \mathcal{T}_h} \int_T \sigma_T (\nabla u - G_T^k \hat{\underline{u}}_T) \cdot \nabla p_T^{k+1} \underline{v}_T, \\ \mathfrak{T}_2 &:= \sum_{T \in \mathcal{T}_h} \sum_{E \in \mathcal{E}_T} \omega_{TE} \int_E \sigma_T (G_T^k \hat{\underline{u}}_T - \nabla u) \cdot n_E (p_T^{k+1} \underline{v}_T - v_{TE}), \\ \mathfrak{T}_3 &:= \sum_{T \in \mathcal{T}_h} \frac{\sigma_T}{h_T} \sum_{E \in \mathcal{E}_T} \int_E (p_T^{k+1} \hat{\underline{u}}_T - \hat{u}_{TE}) (p_T^{k+1} \underline{v}_T - v_{TE}), \\ \mathfrak{T}_4 &:= \sum_{E \in \mathcal{E}_{\Gamma,h}} \int_E \{ \sigma (G_h^k \hat{\underline{u}}_h - \nabla u) \}_{\lambda,E} \cdot n_E [\underline{v}_h]_E, \\ \mathfrak{T}_5 &:= \eta \sum_{E \in \mathcal{E}_{\Gamma,h}} \frac{\alpha}{h_E} \int_E (J_\Gamma - [\hat{\underline{u}}_h]_E) [\underline{v}_h]_E. \end{aligned}$$

We next proceed to estimate the above terms. Using Cauchy–Schwarz inequalities along with the fact that  $\sigma_T \leq \bar{\sigma}$  for all  $T \in \mathcal{T}_h$ , we have for the first term

$$\begin{aligned} \mathfrak{T}_1 &\leq \bar{\sigma}^{1/2} \left( \sum_{T \in \mathcal{T}_h} \|\nabla u - G_T^k \hat{\underline{u}}_T\|_{L^2(T)}^2 \right)^{1/2} \left( \sum_{T \in \mathcal{T}_h} \sigma_T \|\nabla p_T^{k+1} \underline{v}_T\|_{L^2(T)}^2 \right)^{1/2} \\ &\stackrel{(7),(5),(16)}{\lesssim} \bar{\sigma}^{1/2} h^{r+1} |u|_{H^{r+2}(\mathcal{T}_h)} \|\underline{v}_h\|_{\text{en},h}. \end{aligned} \tag{33}$$

For the second term, we use on each edge a  $(2, \infty, 2)$ -Hölder inequality on the integral, the fact that  $\|n_E\|_{L^\infty(E)} \leq 1$  along with  $\sigma_T \leq \bar{\sigma}$ , and a Cauchy–Schwarz inequality on the sums to write

$$\begin{aligned} \mathfrak{T}_2 &\leq \bar{\sigma}^{1/2} \left( \sum_{T \in \mathcal{T}_h} h_T \|G_T^k \hat{\underline{u}}_T - \nabla u\|_{L^2(\partial T)}^2 \right)^{1/2} \left( \sum_{T \in \mathcal{T}_h} \frac{\sigma_T}{h_T} \sum_{E \in \mathcal{E}_T} \|p_T^{k+1} \underline{v}_T - v_{TE}\|_{L^2(E)}^2 \right)^{1/2} \\ &\stackrel{(7),(16)}{\lesssim} \bar{\sigma}^{1/2} h^{r+1} |u|_{H^{r+2}(\mathcal{T}_h)} \|\underline{v}_h\|_{\text{en},h}. \end{aligned} \tag{34}$$

Cauchy–Schwarz inequalities along with  $\sigma_T \leq \bar{\sigma}$  yield for the third term

$$\begin{aligned} \mathfrak{T}_3 &\leq \bar{\sigma}^{1/2} \left( \sum_{T \in \mathcal{T}_h} h_T^{-1} \sum_{E \in \mathcal{E}_T} \|p_T^{k+1} \hat{\underline{u}}_T - \hat{u}_{TE}\|_{L^2(E)}^2 \right)^{1/2} \left( \sum_{T \in \mathcal{T}_h} \frac{\sigma_T}{h_T} \sum_{E \in \mathcal{E}_T} \|p_T^{k+1} \underline{v}_T - v_{TE}\|_{L^2(E)}^2 \right)^{1/2} \\ &\stackrel{(16)}{\lesssim} \bar{\sigma}^{1/2} \left[ \sum_{T \in \mathcal{T}_h} h_T^{-1} \sum_{E \in \mathcal{E}_T} \left( \|p_T^{k+1} \hat{\underline{u}}_T - \gamma_{TE} u\|_{L^2(E)}^2 + \|\gamma_{TE} u - \hat{u}_{TE}\|_{L^2(E)}^2 \right) \right]^{1/2} \|\underline{v}_h\|_{\text{en},h} \\ &\stackrel{(8),(6)}{\lesssim} \bar{\sigma}^{1/2} h^{r+1} |u|_{H^{r+2}(\mathcal{T}_h)} \|\underline{v}_h\|_{\text{en},h}, \end{aligned} \tag{35}$$

where, in the second inequality, we have additionally used the fact that  $(a + b)^2 \leq 2(a^2 + b^2)$  after inserting  $\pm \gamma_{TE} u$  (the trace of  $u|_T$  on  $E$ ) inside the norm. To estimate the fourth term, we start with  $(2, \infty, 2)$ -Hölder inequalities on the integrals and Cauchy–Schwarz inequalities on the sums and recall the definition (17) of  $|\cdot|_{J,h}$  to write

$$\mathfrak{T}_4 \leq \left( \sum_{E \in \mathcal{E}_{\Gamma,h}} \frac{h_E}{\alpha} \|\{ \sigma (G_h^k \hat{\underline{u}}_h - \nabla u) \}_{\lambda,E}\|_{L^2(E)}^2 \right)^{1/2} |\underline{v}_h|_{J,h}. \tag{36}$$

Let now  $E \in \mathcal{E}_{\Gamma,h}$  and, using the inequality  $(a + b)^2 \leq 2(a^2 + b^2)$ , write

$$\begin{aligned}
 & \alpha^{-1} \| \{ \sigma (G_h^k \hat{u}_h - \nabla u) \}_{\lambda, E} \|_{L^2(E)}^2 \\
 & \stackrel{(11)}{\leq} 2 \frac{\lambda_{\text{int}}^2 \sigma_{\text{int}}}{\alpha} \| \sigma_{\text{int}}^{1/2} (G_{T_{\text{int}}}^k \hat{u}_T - \nabla u_{\text{int}}) \|_{L^2(E)}^2 + 2 \frac{\lambda_{\text{ext}}^2 \sigma_{\text{ext}}}{\alpha} \| \sigma_{\text{ext}}^{1/2} (G_{T_{\text{ext}}}^k \hat{u}_T - \nabla u_{\text{ext}}) \|_{L^2(E)}^2 \\
 & \stackrel{(27)}{\leq} \| \sigma_{\text{int}}^{1/2} (G_{T_{\text{int}}}^k \hat{u}_T - \nabla u_{\text{int}}) \|_{L^2(E)}^2 + \| \sigma_{\text{ext}}^{1/2} (G_{T_{\text{ext}}}^k \hat{u}_T - \nabla u_{\text{ext}}) \|_{L^2(E)}^2 \\
 & \stackrel{(7)}{\lesssim} \bar{\sigma}^{-1/2} h^{r+1} |u|_{H^{r+2}(\mathcal{T}_E)}.
 \end{aligned}$$

Plugging the above estimate into (36) and recalling the definition (16) of the energy norm, we conclude that

$$\mathfrak{I}_4 \lesssim \bar{\sigma}^{-1/2} h^{r+1} |u|_{H^{r+2}(\mathcal{T}_h)} \| \underline{v}_h \|_{\text{en}, h}. \tag{37}$$

Moving to the fifth term, we recall that, by (2b),  $J_\Gamma = [u]_\Gamma$  almost everywhere on  $\Gamma$  and use Cauchy–Schwarz inequalities along with the fact that  $\alpha \leq \frac{2\sigma_{\text{int}}\sigma_{\text{ext}}}{2\min\{\sigma_{\text{int}}, \sigma_{\text{ext}}\}} \leq \bar{\sigma}$  and the definition (17) of the  $|\cdot|_{J, h}$ -seminorm to write

$$\begin{aligned}
 \mathfrak{I}_5 & \leq \eta \bar{\sigma}^{-1/2} \left( \sum_{E \in \mathcal{E}_{\Gamma, h}} h_E^{-1} \| [u]_\Gamma - [\hat{u}_h]_E \|_{L^2(E)}^2 \right)^{1/2} | \underline{v}_h |_{J, h} \\
 & \stackrel{(1), (9), (16)}{\lesssim} \bar{\sigma}^{-1/2} \left[ \sum_{E \in \mathcal{E}_{\Gamma, h}} h_E^{-1} \left( \| \gamma_{T_{\text{int}}} E u - \hat{u}_{T_{\text{int}}} E \|_{L^2(E)}^2 + \| \gamma_{T_{\text{ext}}} E u - \hat{u}_{T_{\text{ext}}} E \|_{L^2(E)}^2 \right) \right]^{1/2} \| \underline{v}_h \|_{\text{en}, h} \\
 & \stackrel{(6)}{\lesssim} \bar{\sigma}^{-1/2} h^{r+1} |u|_{H^{r+2}(\mathcal{T}_h)} \| \underline{v}_h \|_{\text{en}, h}
 \end{aligned} \tag{38}$$

Plugging the estimates (33), (34), (35), (37), and (38) into (32), (28) follows.  $\square$

**Proof of Theorem 9.** Straightforward consequence of the Third Strang Lemma [15, Theorem 10] accounting for Lemmas 7 and 13 above.  $\square$

**CRedit authorship contribution statement**

**Daniele A. Di Pietro:** Supervision, Methodology, Conceptualization. **Simon Mendez:** Validation, Supervision. **Aurelio E. Spadotto:** Visualization, Software, Methodology.

**Declaration of competing interest**

The authors declare that they have no known competing financial interests or personal relationships that could have appeared to influence the work reported in this paper.

**Acknowledgements**

Funded by the European Union (ERC Synergy, NEMESIS, project number 101115663). Views and opinions expressed are however those of the authors only and do not necessarily reflect those of the European Union or the European Research Council Executive Agency. Neither the European Union nor the granting authority can be held responsible for them.

The French Région Occitanie is acknowledged for funding part of Aurelio E. Spadotto’s PhD thesis through the 2021-ELEC-CELL project, within the ‘Allocations Doctorales 2021’ call.

The authors are grateful to Prof. Matthieu Hillairet (University of Montpellier) for the precious discussions about the evolutionary potential jump problem described in Section 6.

**Data availability**

Data will be made available on request.

**References**

[1] S. Adjerid, I. Babuška, R. Guo, T. Lin, An enriched immersed finite element method for interface problems with nonhomogeneous jump conditions, *Comput. Methods Appl. Mech. Eng.* 404 (115770) (2023).  
 [2] P.F. Antonietti, S. Giani, P. Houston, *hp*-version composite discontinuous Galerkin methods for elliptic problems on complicated domains, *SIAM J. Sci. Comput.* 35 (3) (2013) A1417–A1439.  
 [3] D. Arnold, *Finite Element Exterior Calculus*, SIAM, 2018.  
 [4] F. Bassi, L. Botti, A. Colombo, D.A. Di Pietro, P. Tesini, On the flexibility of agglomeration based physical space discontinuous Galerkin discretizations, *J. Comput. Phys.* 231 (1) (2012) 45–65.

- [5] L. Beirão da Veiga, A. Russo, G. Vacca, The Virtual Element Method with curved edges, *ESAIM: Math. Model. Numer. Anal.* 53 (2) (2019) 375–404.
- [6] F. Bonaldi, D.A. Di Pietro, J. Droniou, K. Hu, An exterior calculus framework for polytopal methods 3 (2023).
- [7] L. Botti, D.A. Di Pietro, Numerical assessment of Hybrid High-Order methods on curved meshes and comparison with discontinuous Galerkin methods, *J. Comput. Phys.* 370 (2018) 58–84.
- [8] M. Botti, D.A. Di Pietro, M. Salah, A serendipity fully discrete div-div complex on polygonal meshes, *C. R., Méc.* 351 (S1) (2023).
- [9] E. Burman, S. Claus, P. Hansbo, M.G. Larson, A. Massing, Cutfem: discretizing geometry and partial differential equations, *Int. J. Numer. Methods Eng.* 104 (2015) 472–501.
- [10] Erik Burman, Alexandre Ern, An unfitted hybrid high-order method for elliptic interface problems, *SIAM J. Numer. Anal.* 56 (3) (2018) 1525–1546.
- [11] Erik Burman, Alexandre Ern, A cut cell hybrid high-order method for elliptic problems with curved boundaries, in: Florin Adrian Radu, Kundan Kumar, Inga Berre, Jan Martin Nordbotten, Iuliu Sorin Pop (Eds.), *Numerical Mathematics and Advanced Applications ENUMATH 2017*, Springer International Publishing, Cham, 2019, pp. 173–181.
- [12] Erik Burman, Paolo Zunino, A domain decomposition method based on weighted interior penalties for advection-diffusion-reaction problems, *SIAM J. Numer. Anal.* 44 (4) (2006) 1612–1638.
- [13] Andrea Cangiani, Zhaonan Dong, Emmanuil H. Georgoulis, Paul Houston, *hp-Version Discontinuous Galerkin Methods on Polygonal and Polyhedral Meshes*, SpringerBriefs in Mathematics, Springer, Cham, 2017.
- [14] W.H. Coulter, Means for counting particles suspended in a fluid, 1953.
- [15] D.A. Di Pietro, J. Droniou, A third Strang lemma for schemes in fully discrete formulation, *Calcolo* 55 (40) (2018).
- [16] D.A. Di Pietro, J. Droniou, The Hybrid High-Order Method for Polytopal Meshes, in: *Modeling, Simulation and Application*, vol. 19, Springer International Publishing, 2020.
- [17] D.A. Di Pietro, J. Droniou, An arbitrary-order method for magnetostatics on polyhedral meshes based on a discrete de Rham sequence, *J. Comput. Phys.* 429 (109991) (2021).
- [18] D.A. Di Pietro, J. Droniou, A polytopal method for the Brinkman problem robust in all regimes, *Comput. Methods Appl. Mech. Eng.* 409 (115981) (2023).
- [19] D.A. Di Pietro, J. Droniou, F. Rapetti, Fully discrete polynomial de Rham sequences of arbitrary degree on polygons and polyhedra, *Math. Models Methods Appl. Sci.* 30 (9) (2020) 1809–1855.
- [20] D.A. Di Pietro, A. Ern, A hybrid high-order locking-free method for linear elasticity on general meshes, *Comput. Methods Appl. Mech. Eng.* 283 (2015) 1–21.
- [21] D.A. Di Pietro, A. Ern, Arbitrary-order mixed methods for heterogeneous anisotropic diffusion on general meshes, *IMA J. Numer. Anal.* 37 (1) (2017) 40–63.
- [22] D.A. Di Pietro, A. Ern, J.-L. Guermond, Discontinuous Galerkin methods for anisotropic semidefinite diffusion with advection, *SIAM J. Numer. Anal.* 46 (2) (2008) 805–831.
- [23] D.A. Di Pietro, A. Ern, S. Lemaire, An arbitrary-order and compact-stencil discretization of diffusion on general meshes based on local reconstruction operators, *Comput. Methods Appl. Math.* 14 (4) (2014) 461–472.
- [24] D.A. Di Pietro, M.-L. Hanot, M. Salah, Serendipity discrete complexes with enhanced regularity 7 (2024).
- [25] A. Daniele, Pietro Di, Jérôme Droniou, An arbitrary-order discrete de Rham complex on polyhedral meshes: exactness, Poincaré inequalities, and consistency, *Found. Comput. Math.* 23 (2023) 85–164.
- [26] J. Droniou, L. Yemm, Robust hybrid high-order method on polytopal meshes with small faces, *Comput. Methods Appl. Math.* 22 (2022) 47–71.
- [27] E. Du, M. Dao, S. Suresh, Quantitative biomechanics of healthy and diseased human red blood cells using dielectrophoresis in a microfluidic system, *Extrem. Mech. Lett.* 1 (2014) 35–41.
- [28] C. Honrado, P. Bisegna, N.S. Swami, F. Caselli, Single-cell microfluidic impedance cytometry: from raw signals to cell phenotypes using data analytics, *Lab Chip* 21 (1) (2021) 22–54.
- [29] Peiqi Huang, Haijun Wu, Yuanming Xiao, An unfitted interface penalty finite element method for elliptic interface problems, *Comput. Methods Appl. Mech. Eng.* 323 (2017) 439–460.
- [30] August Johansson, Mats G. Larson, A high order discontinuous Galerkin Nitsche method for elliptic problems with fictitious boundary, *Numer. Math.* 123 (4) (2013) 607–628.
- [31] Yoichiro Mori, Y-N. Young, From electrodiffusion theory to the electrohydrodynamics of leaky dielectrics through the weak electrolyte limit, *J. Fluid Mech.* 855 (2018) 67–130.
- [32] E. Neumann, A.E. Sowers, C.A. Jordan, *Electroporation and Electrofusion in Cell Biology*, Springer Science & Business Media, 1989.
- [33] D.A. Saville, Electrohydrodynamics: the Taylor-melcher leaky dielectric model, *Annu. Rev. Fluid Mech.* 29 (1) (1997) 27–64.
- [34] T. Strouboulis, I. Babuška, K. Copps, The design and analysis of the generalized finite element method, *Comput. Methods Appl. Mech. Eng.* 181 (2000) 43–69.
- [35] N. Sukumar, N. Moes, B. Moran, T. Belytschko, Extended finite element method for three dimensional crack modelling, *Int. J. Numer. Methods Eng.* 48 (11) (2000) 1549–1570.
- [36] T. Sun, H. Morgan, Single-cell microfluidic impedance cytometry: a review, *Microfluid. Nanofluid.* 8 (2010) 423–443.
- [37] P. Taraconat, J.-P. Gineys, D. Isèbe, F. Nicoud, S. Mendez, Detecting cells rotations for increasing the robustness of cell sizing by impedance measurements, with or without machine learning, *Cytometry, Part A* 99 (10) (2021) 977–986.
- [38] Pierre Taraconat, Jean-Philippe Gineys, Damien Isebe, Franck Nicoud, Simon Mendez, Numerical simulation of deformable particles in a coulter counter, *Int. J. Numer. Methods Biomed. Eng.* 35 (11) (2019) e3243.
- [39] Pierre Taraconat, Jean-Philippe Gineys, Damien Isebe, Franck Nicoud, Simon Mendez, Red blood cell rheology during a complete blood count: a proof of concept, *PLoS ONE* 18 (1) (2023) e0280952.
- [40] Geoffrey Ingram Taylor, Studies in electrohydrodynamics. I. The circulation produced in a drop by an electric field, *Proc. R. Soc. Lond. Ser. A, Math. Phys. Sci.* 291 (1425) (1966) 159–166.
- [41] Petia M. Vlahovska, Electrohydrodynamics of drops and vesicles, *Annu. Rev. Fluid Mech.* 51 (2019) 305–330.
- [42] L. Yemm, A new approach to handle curved meshes in the hybrid high-order method, *Found. Comput. Math.* 24 (2024) 1049–1076.